ANALYZING DUCTILE SHEAR ZONE NETWORK GEOMETRIES IN THE GRASSY PORTAGE SILL, RAINY LAKE REGION, NORTHWESTERN ONTARIO, CANADA

by

Ernest J. Thalhamer

A Thesis Submitted in

Partial Fulfillment of the

Requirements for the Degree of

Master of Science

in Geosciences

at

The University of Wisconsin-Milwaukee

December 2018

ABSTRACT

ANALYZING DUCTILE SHEAR ZONE NETWORK GEOMETRIES IN THE GRASSY PORTAGE SILL, RAINY LAKE REGION, NORTHWESTERN ONTARIO, CANADA

by

Ernest J. Thalhamer

The University of Wisconsin-Milwaukee, 2018
Under the Supervision of Dr. Dyanna Czeck

The Grassy Portage Sill (GPS) is a ~2.7 Ga metagabbroic sill located in the Rainy Lake region of northwestern Ontario. The Rainy Lake region is located in the Superior Province between the metavolcanic Wabigoon subprovince to the north and the metasedimentary Quetico subprovince to the south. Two regional faults bound the region and intersect to the east, forming a wedge which defines the Rainy Lake zone. This area was regionally deformed due to oblique transpression, resulting from the Kenoran Orogeny (~2.7 Ga). The GPS is approximately 20 km long and 1-2 km wide, and has undergone heterogeneous strain along its length. This strain variation is a function of the competence contrast between the GPS, the gneissic Rice Bay Dome to the west, and the metavolcanic and metasedimentary units between the two. The GPS has a higher competence than the adjacent metavolcanic and metasedimentary units, but all have a lower competence than the Rice Bay Dome. Within the GPS, anastomosing ductile shear zone networks accommodated the bulk of the deformation within the largely competent sill. The orientations of the networks vary along the length of the sill, apparently related to strain variations, as the inferred shortening directions of the shear zone networks matches those assumed from regional foliations and calculated from previous work on deformed dikes and veins. At all locations, both steeply dipping dextral and sinistral sets of shear zones formed,

presumably simultaneously as evidenced by mutual cross-cutting relationships. The shear zones are curviplanar and dip more shallowly near some of their intersections. The style of deformation varies within the gabbro based on grain size. Fine grained lithologies are deformed via a pervasive foliation. Coarser grained lithologies generally contain discrete (mm-cm scale) shear zones, often without a pervasive foliation. There is no relationship between mineralogy and shear zone or foliation formation. Microstructural analysis of shear zone bearing samples indicated that dislocation creep served as the primary deformation mechanism throughout the GPS, but showed no pattern regionally, or with grain size. At the lowest strain sites, the gabbro has a pervasive foliation, but few, if any, shear zones. At low-medium strain sites, the sinistral and dextral shear zone sets have fairly consistent orientations, approximately 65-75° apart from one another. As strain increases, the orientations of both sets become increasingly more variable and the average angle between the two sets decreases. We hypothesize that the shear zone sets formed at relatively high angle to one another and rotated to a lower relative angle with increasing strain. The newer strands in the higher strained sites formed at high angle, causing the orientations of each shear zone set to become more diffuse at higher strain.

TABLE OF CONTENTS

LIST OF FIGURES

LIST OF TABLES

ACKNOWLEDGEMENTS

I am deeply grateful to my advisor Dr. Dyanna Czeck. Without her knowledge, assistance, and guidance, I would have never completed this project. Her mentorship has made me into a better scientist, and her faith in me has made this all possible. I am also thankful to Dr. Lindsay McHenry and Dr. Barry Cameron, for their insight and expertise throughout this entire process. Additionally, I want to thank Dr. Elena Druguet and Dr. Jordi Carreras. They have served as a constant source of knowledge and advice, and their previous work in the region was crucial to my own.

To the scientists from my past who helped set me down the path on which I find myself today. Dr. Gary Solar, my undergraduate mentor and friend, you brought me into your lab and taught me how to be a researcher. Even more, you helped me to understand that there were unanswered questions in the world, and gave me the tools to answer them. Also to Mr. Chris Visco, whose high school classroom I stumbled into, at a time where I had written off science completely. Thank you for infecting me with your passion, which you warned us all, though I had no idea it would take me this far.

For my father, no words can express how important you have been and how much your support has meant to me. You have allowed me to pursue my passions, and supported me in more ways than I can ever recount, or thank you enough for.

I would like to thank Kiel Finn, whose assistance in the field helped to set this project off on the right path. Also, I want to acknowledge the University of Wisconsin-Milwaukee Geosciences department, the ILSG, and the Precambrian Research center for their financial support of the project.

Lastly and most importantly, I want to thank my wife Haylee, for her constant love and support. She has made countless sacrifices to allow me to complete this project and it would not have happened without her.

Chapter 1: Introduction

1.1 Shear Zones

Shear zones, and their brittle equivalent, faults, are common and important structural features that are indicative of inhomogeneous deformation in the crust. Near the surface, deformation is typically accommodated by brittle processes including faulting, whereas ductile shear zones accommodate deformation at depth. A variety of factors including pressure, temperature, strain rate, rock type, and presence and type of fluids control the transition between brittle and ductile deformation styles with depth. Faults and shear zones can both accommodate offsets from the sub millimeter to the multi-kilometer scales.

Ductile shear zones are typically defined as planar bands of highly deformed rock, surrounded by lesser to undeformed rock, where offset is localized without a loss of continuity at the macroscopic scale (Fossen, 2010). More often, shear zones are not found in discrete planar bands, but rather in more complex curvilinear geometries which link with others to form complex anastomosing geometries that bound undeformed or lesser deformed lozenges (Ramsay and Graham, 1970; Mitra, 1979, 1998; Ramsay and Allison, 1979; Bell, 1981; Choukroune and Gapais, 1983; Gapais et al., 1987; Burg et al., 1996; Corsini et al., 1996; Hudleston,1999; Arbaret et al., 2000; Carreras, 2001; Czeck and Hudleston, 2003, 2004; Pennachioni, 2005; Fusseis et al., 2006; Bhattacharyya and Czeck, 2008; Carreras et al., 2010).

1.2 Ductile Shear Zone Networks

Often, shear zones are not found as individual strands, but instead are interconnected into more complex networks, often in conjugate pairs (Fig. 1a & 1b) (e.g. Ramsay and Allison, 1979; Bell, 1981; Choukroune and Gapais, 1983; Gapais et al., 1987; Burg et al., 1996; Burg, 1999;

Hudleston, 1999; Arbaret et al., 2000; Carreras, 2001; Arbaret and Burg, 2003; Burg et al., 2005; Bhattacharyya and Czeck, 2008; Carreras et al., 2010; Ponce et al., 2013). These networks of conjugate pairs are often curviplanar and bound larger bodies, or lozenges, of lesser or undeformed rock. Anastomosing shear zone networks are important because: 1) their geometries have been called upon to explain the mechanical processes that initiate shear zones (e.g. Fusseis et al., 2006) and, 2) their patterns help explain strain accommodation while maintaining strain compatibility (e.g. Hudleston, 1999). The formation and development of brittle shear fracture networks are well-studied (e.g. Wilcox et al., 1973; Ackermann and Schlische, 1997; Maerten et al., 2002), but similar ductile shear zones studies are relatively scarce.

A variety of models have been proposed to explain the initiation and development of shear zones, and shear zone networks. Pennacchioni and Mancktelow (2007) proposed that shear zones form along preexisting brittle structures, and that the transition is always from brittle to ductile (Segall and Pollard, 1983; Pennachioni and Mancktelow, 2007; Fusseis et al., 2006; Goncalves et al., 2016). Geometry would therefore be controlled by the orientation and distribution of brittle structures, which is a testable hypothesis since the geometry of brittle structures is relatively well known. A second model proposes that ductile shear zones initiate at sites of preexisting instabilities within the rock, and that these microscopic flaws alone are sufficient for shear zones to initiate (Hobbs et al., 1990; Ingles et al., 1999; Mancktelow, 2002; Mandal et al. 2004; Misra and Mandal, 2007) or at the larger scale such as localization along weaker phases (e.g. Christiansen and Pollard, 1997).

To date, many researchers have studied the geometry and evolution of shear zone networks in the field (Mitra, 1979; Bell, 1981; Gapais et al., 1987; Carreras, 2001; Carreras et al., 2010) and in numerical experiments (Cobbold et al., 1971; Hudleston, 1999; Mancktelow,

2002; Mancktelow, 2006). Although there has been extensive work on studying the geometries of developed shear zone networks, there is a lack of understanding on how and why shear zone strands initiate and evolve to form these complex anastomosing networks. Results from numerical based experiments indicate that conjugate shear zone pairs within networks often initiate in approximately perpendicular orientations and rotate with continuous deformation (Mancktelow, 2002). However, in the field setting, these histories are far more elusive.

Carreras et al. (2010) observed sets of conjugate shear zones in a single high-strained gabbro outcrop and developed criteria to determine the relative timing of the shear strands in order to unravel their geometrical development and rotational histories. Using field measurements a model was derived to explain the sequential development of shear zone networks within the site (Fig. 2). In the early stage of deformation, conjugate sets of shear zones develop, with dextral and sinistral strands which are oriented at an approximately 90° orientation, which faces the bulk shortening direction (Z in Fig. 2). In later stages, the shear zone strands formed during earlier stages will rotate relative to the bulk shortening orientation, as well as become thicker under progressive deformation. Using this model, they could interpret an inferred shortening direction and estimate the approximate strain magnitude.

For a shear zone to maintain compatibility, or coherence during deformation, across its borders, it must remain continuous across the boundary between the deformed shear zone and the non-deformed outlying rock. During simple shearing this compatibility is maintained but, when a component of pure shearing or flattening is added, for example during transpression, there must be an associated volume loss or extrusion of material. Complex shear zone networks have been called upon as a way for strain to be accommodated while maintaining compatibility

when there is no loss of volume in the shear zone (Hudleston, 1999) and no escape from the system for large-scale extrusion to take place (Baird and Hudleston, 2007).

The relationships between shear zone thickness, displacement, and duration of deformation have also been studied. In some field examples, shear zone thickness can be considered roughly proportional to age (Mitra, 1979; Carreras et al., 2010), which indicates shear zones widen over time. Indeed, an analysis of shear zone displacement as compared to thickness from a variety of tectonic settings showed a correlation between thicker shear zones and greater displacement, further supporting thickness as a viable measure of relative deformation duration (Fossen and Cavalcante, 2017). However, the details of this relationship are affected by rock rheology, especially strain softening or hardening (Hull, 1988; Means,1995; Schrank et al., 2008) and history of brittle displacement in early or intermittent deformation stages (Pennacchioni, 2005; Fusseis et al., 2006; Fossen and Cavalcante, 2017). Therefore, the general rule that thicker shear zones accumulated more displacement and therefore recorded a longer duration of deformation is likely to be true, but should be used with caution.

1.3 Grassy Portage Sill Shear Zones

Shear zones for this study are located within the Grassy Portage metagabbroic sill (GPS), the same unit studied by Carreras et al. (2010) for their detailed analysis. The GPS is located in the Rainy Lake region at the Quetico/Wabigoon subprovince boundary of North America's Superior Province (Fig. 3). Shear zones, which range from mm to cm scale in width, are present at the majority of studied outcrops within the sill. The GPS shear zones were chosen for this

study due to their extent and variation. Strain magnitude is heterogeneous within the sill. This strain gradient allows evaluation of shear zone network development with increasing strain.

The region has undergone dextral transpression deformation, which has been expressed in a variety of ways including homogenous strain evidenced by a single penetrative fabric and flattening strains, distributed structures which accommodate the dextral motion and flattening strains separately such as strike-slip shear zones and folds, or strongly localized shear zones cutting otherwise undeformed units. These different styles of deformation are primarily due to lithological variations, relative competence contrasts, and structural variations of the metasedimentary, metavolcanic units, and plutonic units (Poulsen, 2000; Czeck and Hudleston, 2003; Czeck et al. 2006; Druguet et al. 2008; Czeck et al. 2009; Bauer et al., 2011). The deformation in the GPS has yet to be studied in detail and placed into this larger context.

1.4 Study Goals

My goals for this study are three-fold. First, through a detailed geometric analysis, I will determine the evolution of shear zones across a strain gradient. Second, I will constrain the lithological variations, including mineralogy and grain size, to determine their effects on strain patterns and shear zone formation. Last, I will conduct a quantified microstructural analysis to interpret the underlying deformation mechanisms responsible for the strain patterns. The importance of this work is that it will help us understand how individual shear zone strands form and develop into complex anastomosing shear zone networks.

This work will also help us understand the regional deformation by defining the kinematics and localized deformation variations within this understudied unit. The deformation

within the GPS will be placed within the larger context of deformation in the Rainy Lake region to help explain how deformation is partitioned into this relatively small, strong rock unit.

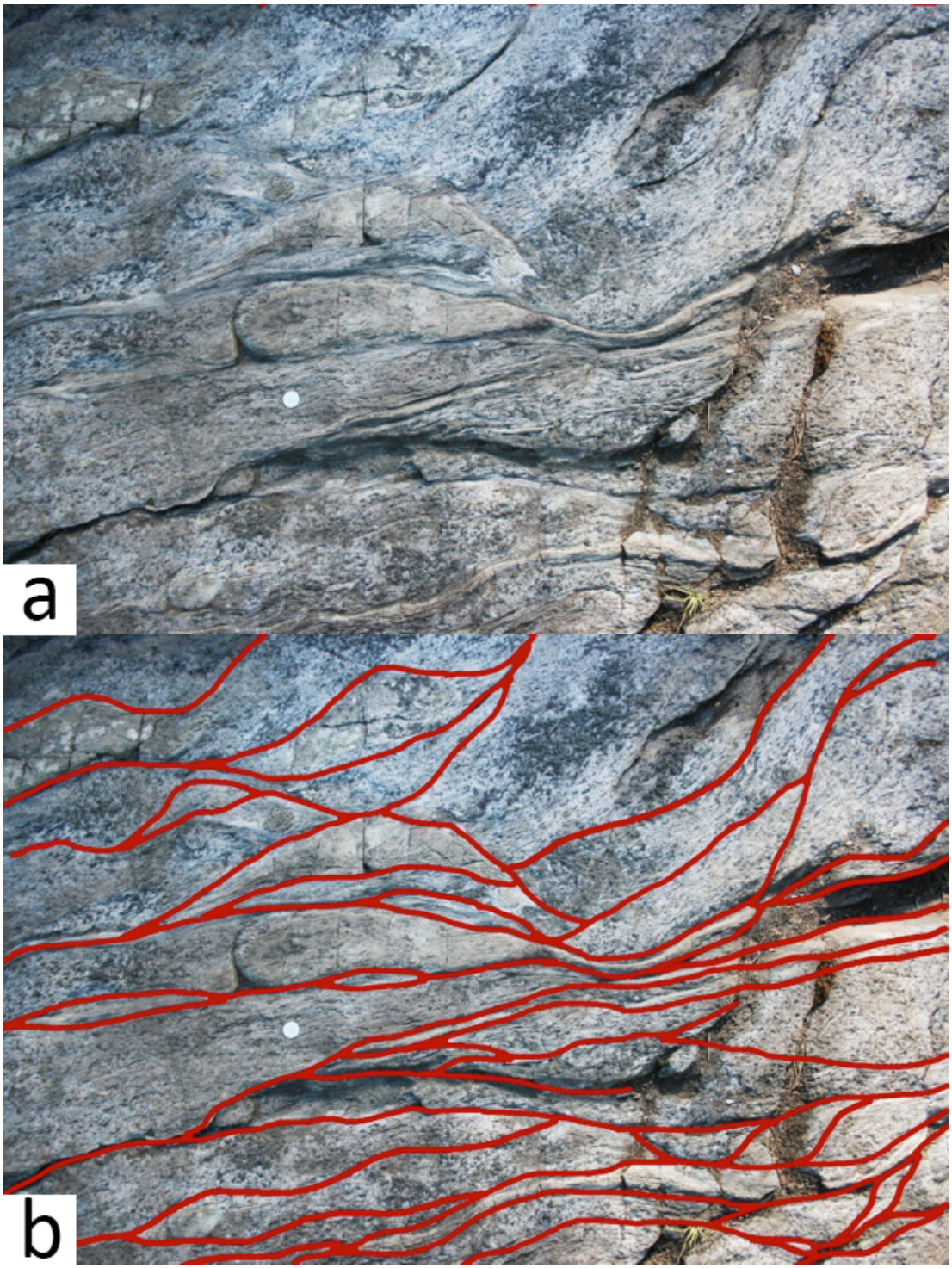

Figure 1: (a) Photograph of the anastomosing shear zone network within metagabbro on subhorizontal plane at site from Carreras et al. 2010 study (coin for scale). This site is located adjacent to Site 7 on the map shown on Figure 6. Shear zones are defined by narrow zones of intense foliation surrounding undeformed lozenges and display an anastomosing network pattern. **(b)** Same photograph as displayed in (a), with shear zones traced in red.

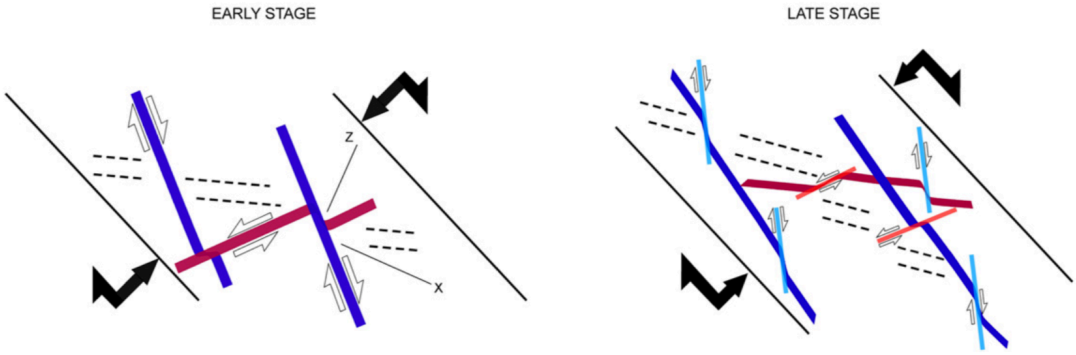

Figure 2. Model for the sequential development of shear zones from Carreras et al. 2010. In the early stage, dextral and sinistral shear zones initiate at an approximate 90° orientation facing the bulk shortening direction (Z). Through progressive deformation, these initial shear zones rotate in opposing directions, increasing the angle between them, while near shear zones initiate at the ~90° orientation, leading to their complex modern geometries.

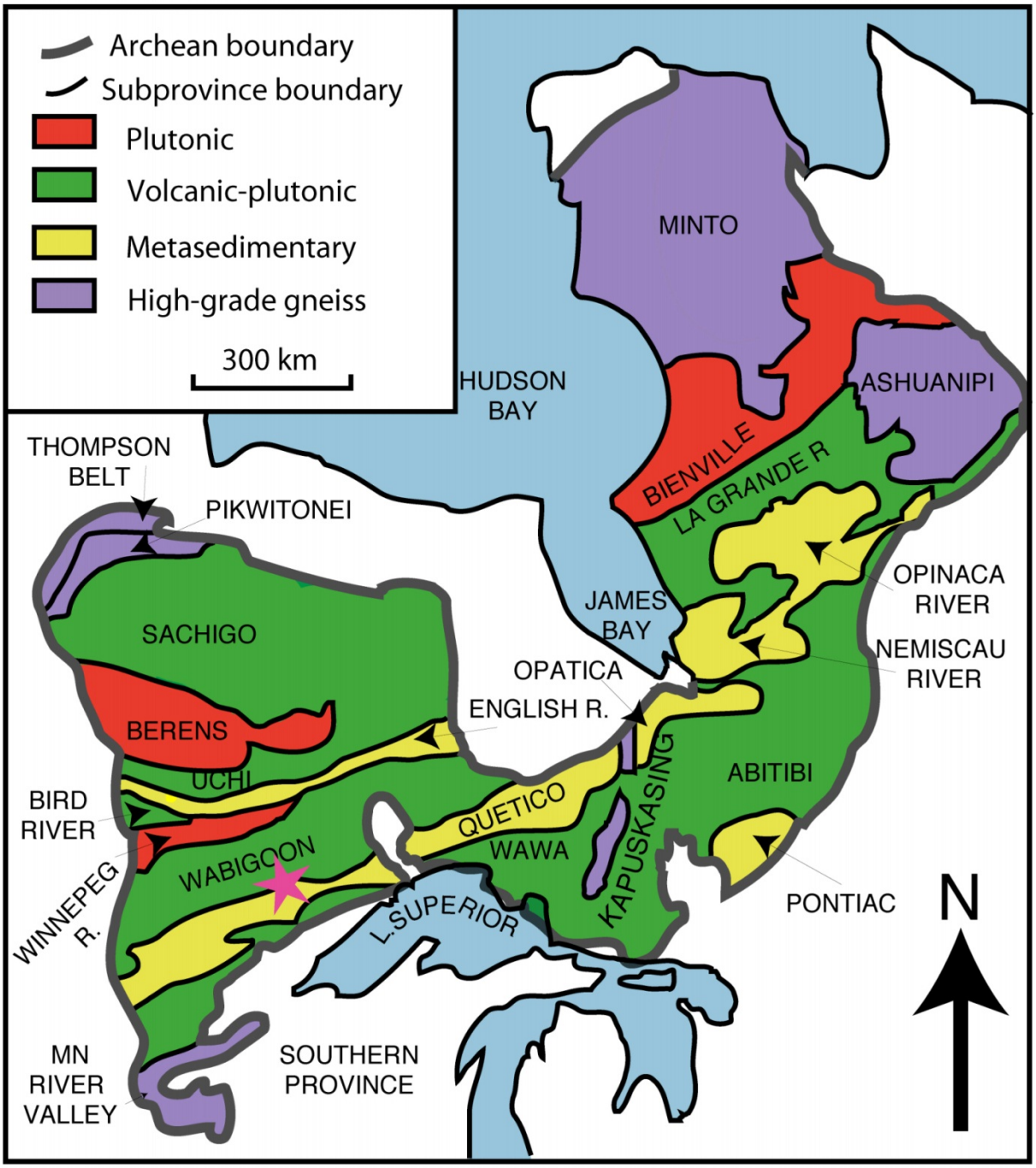

Figure 3: The Superior Province. From Czeck and Hudleston (2003), modified from Card & Ciesielski (1986). Location of study indicated by star.

Chapter 2: Geologic History

2.1 Geological History of the Superior Province

The Superior Province covers an area of over 2 million km^2 and represents the world's largest exposed undisturbed body of Archean aged rock (Card and Ciesielski, 1986; Fig. 3). After its initial Archean formation and deformation, the central part of the Superior Province has been relatively undisturbed since ~2.6 Ga, making it a desirable location to study Archean tectonic history.

The Superior Province is subdivided into a series of subprovinces based on their lithologic assemblages (Card and Ciesielski, 1986). The central subprovinces are either metavolcanic/plutonic (granite-greenstone) or metasedimentary lithologies. The metavolcanic/plutonic subprovinces are most commonly interpreted to have formed by the accretion of a series of island arcs (Langford and Morin, 1976; Percival and Williams, 1989; Card, 1990). The metavolcanic/plutonic subprovinces formed as arcs, and the metasedimentary subprovinces formed from adjacent accretionary prisms. Consistent with this interpretation, within the arc sequences, ages are similar along strike, but vary significantly across it (Hoffman, 1989).

The late Archean Kenoran orogeny occurred at ~2.7 Ga and assembled the central Superior Province. During the Kenoran, island arcs formed, and subsequent subduction led to arc collision. Deformation within the Rainy Lake region is a result of oblique arc collisions, resulting in transpressional deformation which partitioned differently within the various rock units. Greenschist (east) to amphibolite (west) facies metamorphism accompanied deformation (Poulsen et al., 1980; Davis et al., 1989; Poulsen, 2000; Druguet et al., 2008).

2.2 Geological History of the Rainy Lake Region

The boundary between the Quetico and Wabigoon subprovinces is characterized by a sharp change in lithology and localized deformation. The Rainy Lake Region is a structurally bounded triangular wedge, located between the metasedimentary Quetico (south) and metavolcanic/plutonic Wabigoon (north) subprovinces near the area of International Falls, Minnesota and Fort Frances, Ontario (Fig. 4). This wedge is bound by the Quetico fault at its northern boundary and the Seine River-Rainy Lake fault at its southern boundary. The bounding faults have likely served as both faults and shear zones at different times throughout their history (Czeck and Fralick, 2002).

Lithologically, the Rainy Lake Region has similarities to both the Wabigoon and Quetico subprovinces. Within the zone, this oblique convergence was accommodated by north-south oriented shortening accompanied by dextral strike-slip motion, resulting in a dextral transpressive deformation regime. This is evidenced regionally by subvertical foliations and asymmetric features in subhorizontal planes coinciding with dextral shear (Poulsen, 1986; Poulsen, 2000; Czeck and Hudleston, 2003; Druguet et al., 2008; Czeck et al., 2009; Bauer et al., 2011; Fernández et al., 2013).

Five general lithologic units in the Rainy Lake Region have been defined based on previous studies (Lawson, 1887, 1913; Poulsen, 2000) in addition to ages obtained by Davis et al. (1989) and Fralick and Davis (1999):

1. Metavolcanic rocks (Keewatin Group, 2728 ± 4 to 2725 ± 2 Ma): vary from ultramafic to felsic composition, found in layered sequences.

2. Metasedimentary rocks (Coutchiching Group, between 2704 ± 3 and 2692 ± 2 Ma based on detrital zircon and a cross-cutting intrusion): metapelites and metagreywackes, predominantly biotite schist, interpreted to be accretionary prisms.
3. Metagabbroic rocks (2728 – 2727 Ma): variably sized sills, ranging from melagabbro to anorthosite composition. Grassy Portage Sill is one of the largest examples in the region.
4. Gneisses (2725 ± 2 Ma: Medium to coarse grained, commonly foliated or lineated, granitic gneiss and paragneiss with local occurrence of mica schist, mafic schist, and quartz-feldspar porphyry. Rice Bay Dome is one of the largest examples in the region.
5. Granitoids (2686 ± 2 Ma): Relatively undeformed, medium- to coarse-grained quartzofeldspathic granite, granodiorite, and quartz monzonite plutons. These have been demonstrated to have formed syntectonically, late within the Archean transpressional event (Czeck et al. 2006).

Two major deformation phases formed the structures within the Rainy Lake Region (Poulsen, 1986; Davis et al. 1989; Poulsen, 2000). The first phase of deformation (D_1) involved faulting and recumbent folding of both the island arc and the accretionary prism units resulting in the modern day inversion of all strata (Poulsen et al., 1980; Borradaile, 1982; Poulsen, 2000a). It was during this deformation that a regional schistosity was developed (S_1) which is subparallel to the meta-volcanic and meta-sedimentary rocks.

Subsequent to the stacking of units during D_1 deformation, many surficial units were buried and deformed during the second deformation event (D_2). D_2 is characterized by a shift in deformation to folding and dextral transpression. It is during this deformation event that the

strong deformational fabrics found throughout the Rainy Lake region formed, including those within the GPS (Czeck & Hudleston, 2003; Bauer et al. 2011). The deformation during this second phase manifested differently as discrete or distributed structures, dependent on the competence of the unit (Druguet et al. 2008; Bauer et al. 2011).

2.3 The Grassy Portage Sill

Shear zones for this study are located within the Grassy Portage sill (GPS), an overturned, steeply dipping gabbroic intrusion (Fig. 5). The GPS "wraps" around the gneissic Rice Bay Dome, and is exposed over an approximate 20 km long and 1-2 km wide area. Bound between the Rice Bay Dome to the northwest and the GPS to the southeast, is a layered rock sequence largely consisting of Keewatin metavolcanic rocks ranging from intermediate to ultramafic with some interlayered metasedimentary rocks largely consisting of biotite schist. At the southeastern contact of the GPS is a similar layered sequence, largely composed of Coutchiching biotite schist, which contains multiple late granitic intrusions, with minor mafic metavolcanic layers.

The GPS is primarily composed of metagabbro ranging from leucogabbro to gabbro in composition. It contains layers defined both compositionally and mineralogically that may have formed by gravitational settling or auto intrusion (Poulsen, 2000). Layering occurs at scales from centimeter to kilometer. The GPS is primarily composed of plagioclase, which is likely of igneous origin, and hornblende, which is likely metamorphically derived. At the base of the GPS (west side) is a hornblende-rich coarse-grained melagabbro. Moving across strike, there is a decrease in grain size and increase in plagioclase content, with the finest grained gabbros found at the top of the GPS (easternmost exposures). Grain size variation is extensive at both a micro and macroscopic scale (Fig. 6). The sill also contains anorthositic lenticular pods within the

gabbros. Davis et al. (1989) performed U/Pb zircon dating using a sample from the upper part of the intrusion, and yielded an age of 2724 +/- 2 Ma.

The GPS has been extensively studied for its potential economic uses due to its sulfide and oxide mineralization, which has been actively mined for chalcopyrite and pyrrhotite (Poulsen, 2000). Lenses of pyrrhotite-chalcopyrite, ranging from disseminated to massive, can be found at the base. In addition, stringers and disseminations are found within a siliceous member of the upper zone and in and near gabbroic dikes crosscutting the adjacent mafic and ultramafic units.

Centimeter-scale shear zones are found within the gabbro, sometimes localized at lithological boundaries between the gabbro and anorthositic pods. The shear zones primarily have strike slip shear sense, with both dextral and sinistral oriented motion, and are observed on the subhorizontal plane. Additionally, shear zones were localized at some of the unit boundaries. In particular, the southern contact is sheared where exposed (Davis et al., 1989), but metasedimentary inclusions within the GPS suggest that it was intruded as a sill between the Keewatin and Coutchiching groups (Davis et al., 1989), and that the shearing merely modified this boundary.

Previous studies within the region (Poulsen, 2000) and within the GPS (Carreras et al. 2010) indicate that shear zones are a common occurrence within multiple units in the region, including the gneisses and metagabbroic sills. The shear zones are centimeters to meters in width and, in some regions, contain quartz and are gold bearing. Within the GPS, a weak pre-shearing foliation was observed, which showed continuity with the regional foliation (Carreras et al., 2010).

The heterogeneous strain within the GPS is likely a function of the competence contrast between the sill, the gneissic dome, and the metavolcanic and metasedimentary rocks lying between the two units (Bauer et al., 2011). The GPS has a higher competence than the adjacent metavolcanic and metasedimentary units, but all of these units have a lower competence than the Rice Bay dome. The competence contrasts result in a regional scale strain shadow created by the strong Rice Bay Dome, which was partially resistant to regional deformation (Druguet et al., 2008; Carreras et al., 2010; Bauer et al., 2011;Block, 2014).

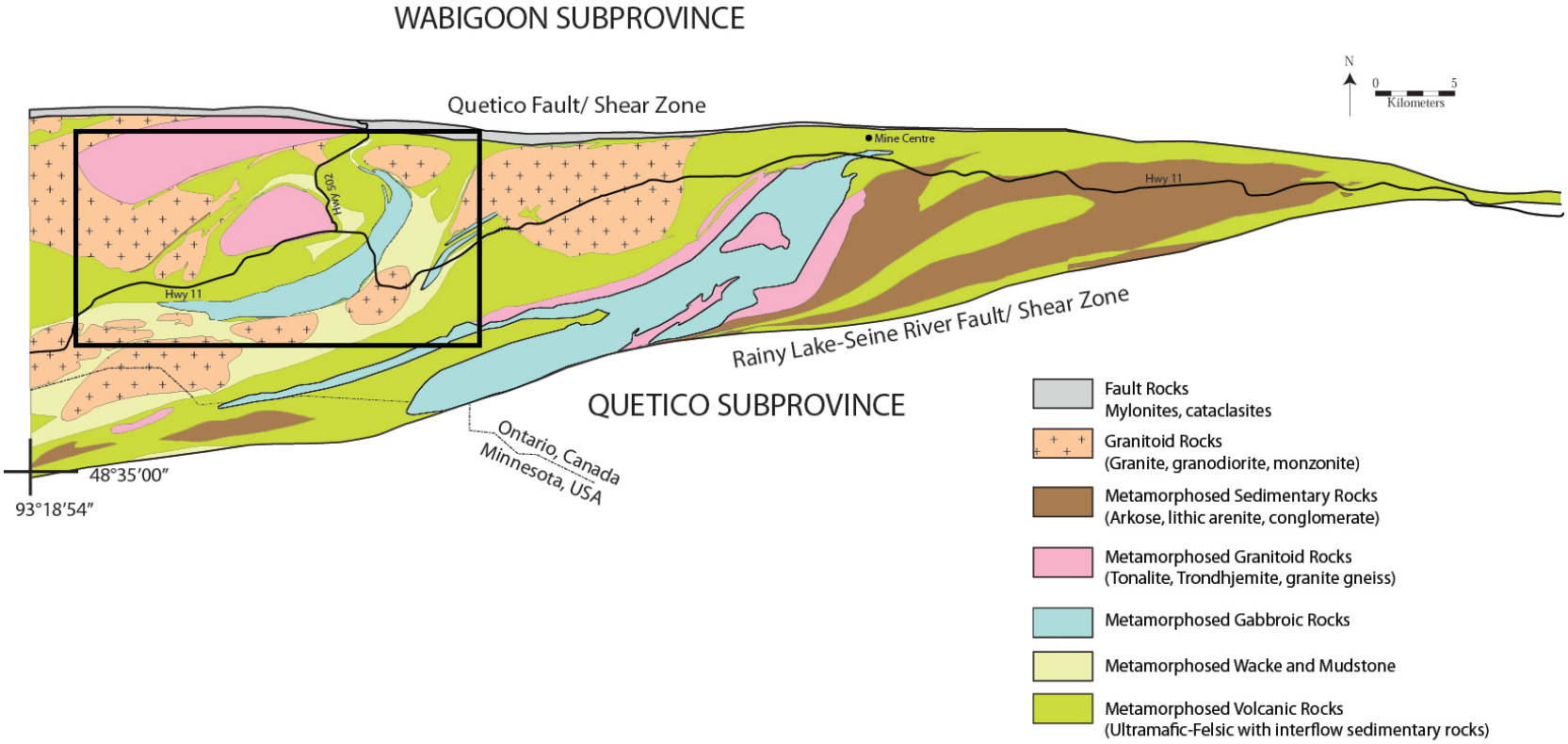

Figure 4. The Rainy Lake region is bounded to the north by the Quetico Fault/Shear Zone and to the south by the Rainy Lake-Seine River Fault/Shear Zone. This wedge forms the boundary between the Wabigoon and Quetico subprovinces. Area in box shown in greater detail in Fig. 4. Geology is simplified, combined, and modified by Bauer et al., 2011. Geology from Wood et al. (1980a, 1980b), Davis et al. (1989), Stone et al. (1997a, 1997b), and Poulsen (2000).

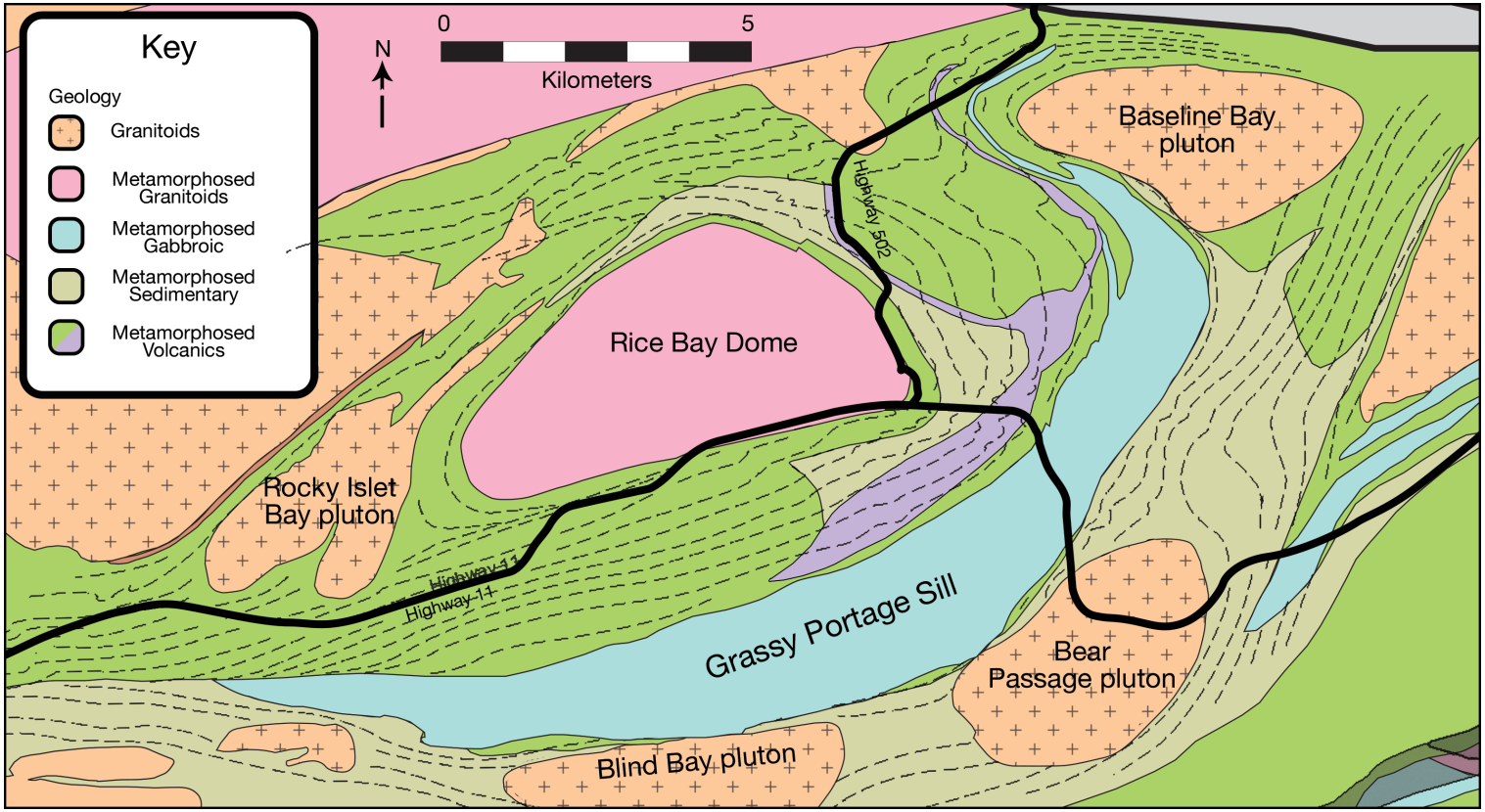

Figure 5. Simplified geologic map of the Grassy Portage Sill and surrounding geology. Modified from Druguet et al., 2008 based on from Davis et al. (1989) and Poulsen (2000).

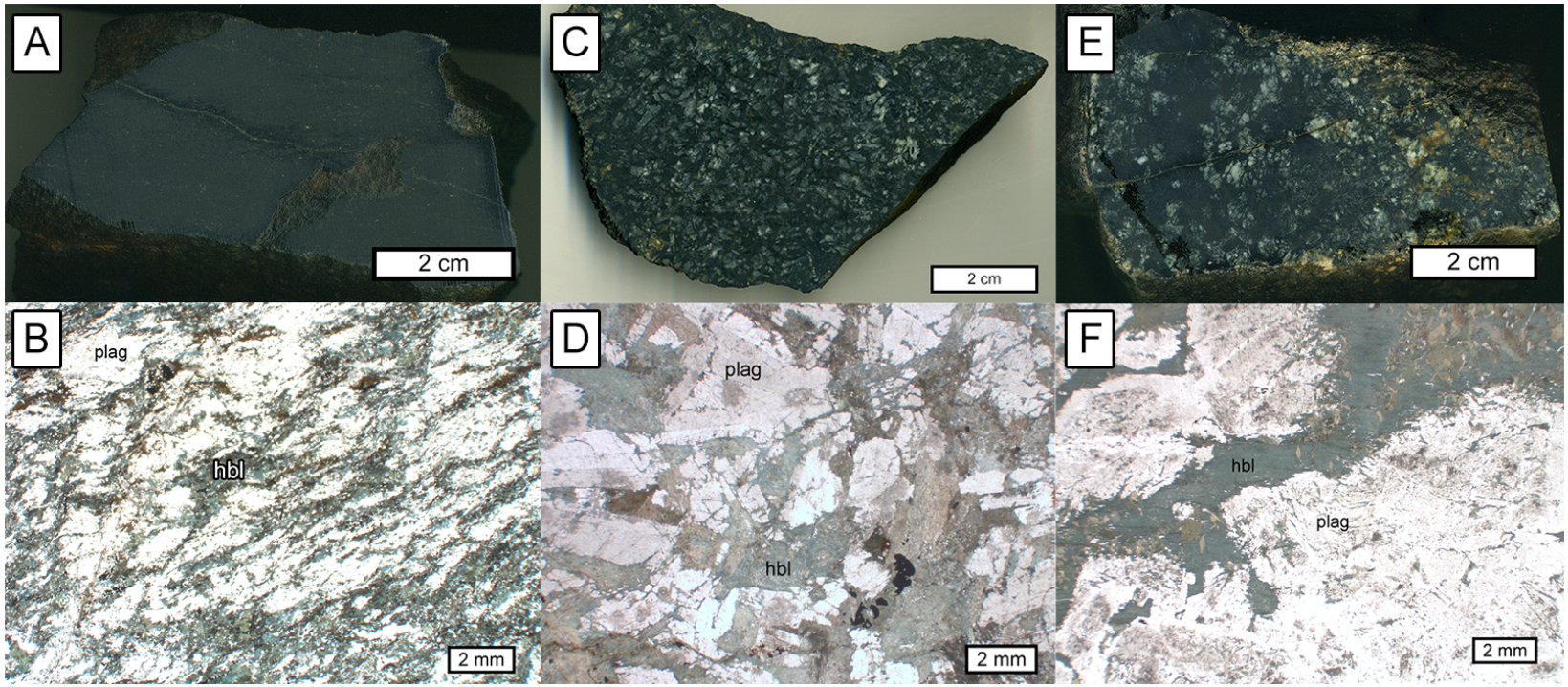

Figure 6. (A) Hand sample from GPS11-04 (low strain) with very fine grain size **(B)** Photomicrograph from sample in (A), from XZ plane (Plane parallel to lineation and perpendicular to foliation), which displays pervasive foliation at micro- scale **(C)** Hand Sample from GPS11-03 (medium strain) **(D)** Photomicrograph from sample in (C), from XY plane **(E)** Hand sample from GPS11-07 (high strain) **(F)** Photomicrograph from sample in (E), from XY plane. Locations shown on Fig. 6.

Chapter 3: Methods

3.1 Field Methods

Study sites were selected in the Grassy Portage Sill based upon availability of outcrop and spatial separation. To be useful for this study, an outcrop needed multiple exposed dimensions and relatively clean (free of lichen) surfaces to make it possible to identify the sub centimeter shear zones. While many of the natural outcrops lacked these criteria, there were three zones within the GPS which fit both criteria. These were: 1) The Northern region, an inactive but recently logged area, 2) The Central Region, along Highway 11 and an adjacent power line cut, and 3) The Southern Region, an abandoned mining camp. There were several good outcrops within each of these zones (Fig. 7). Field observations included estimates of grain size, mineralogy, and structural fabric measurements. Primary fabrics included foliation and lineation, which were defined by the alignment of mafic minerals, predominately hornblende.

Next, I measured the individual shear zones including the orientation of the shear zone plane, shear zone thickness, and deflection of mineral (typically hornblende) orientations across the shear zones. Mineral deflection indicates sense of shear, dextral or sinistral motion (Fig. 8). Not all shear zones had a clearly defined sense of motion, in which case they were identified as ambiguous.

The last step at each outcrop was a qualitative assessment of the strain magnitude in order to compare sites. This qualitative assessment was done by observing the foliation intensity and the density of shear zones at the site in addition to grain size, presence of fabric, and shear zone thickness. Sites were assigned a broad label (low, medium-low, medium, medium-high, or high) to describe their strain magnitude.

Previous studies indicated the presence of fine-grained lenticular pods of anorthosite within the GPS (Poulsen, 2000; Carreras et al. 2010). In lower strain interpreted exposures these pods are equant in shape. Within higher strained rocks, they become flattened/ellipsoidal with progressive deformation. As such, these pods could theoretically be used as strain markers within the GPS. Where present, long and short axes dimensions of anorthositic pods on sub-horizontal surfaces were measured, to determine their strain.

3.2 Shear Zone Analysis

Shear zone orientations, separated into dextral and sinistral strands, were plotted onto stereographic projections, based upon their outcrop site (Fig. 9), and separated based on shear zone thickness. The mean vector, or average orientation, for each set (dextral and sinistral), was calculated. Lastly, I measured the obtuse angle between the two average strand orientations. Previous work suggested that conjugate shear zones initiate at ~90 degree angles (Ramsay and Graham, 1970), and with progressive deformation, the angle between the two limbs that face the mean shortening direction may increase (Z in Fig. 9; Mitra, 1979; Ramsay and Huber, 1987). Carreras et al. (2010) performed a kinematic analysis at a single site within the Grassy Portage Sill, and concluded that the conjugate shear zones were consistent with that pattern of initiation and evolution.

The intermediate Y direction was found at the intersection between the mean conjugate shear zones. The X (maximum extension) and Z (maximum shortening) directions were found on the plane perpendicular to Y, each bisecting the angles between conjugate shear zones, with Z bisecting the obtuse angle and X bisecting the acute angle.

3.3 Thin Section Analysis

Eight oriented samples were collected from 7 sites. These samples were chosen to be representative across lithological variation and inferred strain magnitude. From these 8 samples, 22 thin sections from the principal planes of finite strain were created. I was able to generate X-Y and X-Z planes from all samples, and most had a Y-Z oriented thin section as well (using convention that finite strain axes X>Y>Z where X is the lineation orientation and XY plane is the foliation plane).

The X-Y thin section of each sample was used for the quantitative analysis, totaling 8 sections. Before performing the quantitative thin section study, I performed a qualitative inspection of all thin sections to assess the minerals and microstructures that were present. The lists of those minerals and microstructures were used in the quantitative analysis.

At 200 points along a grid within each thin section, I recorded the mineral type, the long and short axes lengths of the grain, and the microstructures present. Plagioclase is the primary microstructure-bearing mineral; other minerals appeared resistant to deformation. Therefore, I plotted the long axis length data from plagioclase for each site on histograms (Fig. 17-19). Except for some recrystallized grains found primarily along rims of original plagioclase grains, plagioclase grain sizes are retained from the igneous protolith. They are roughly equivalent in size to amphibole grains which are metamorphic in origin, suggesting that the metagabbro grain size distribution is related to the original igneous grain size heterogeneity and maintained through metamorphism. Additionally, I calculated an approximate average grain size of each sample across all minerals by taking the average of the long axis multiplied by the short axis of each grain.

Lastly, I quantified plagioclase microstructure data and grouped them based on the interpreted deformation processes. Microstructures found within the Grassy Portage Sill were likely derived from four interpreted deformation processes: brittle, crystal plastic, crystal plastic recovery, and alteration (Fig. 10). The majority were observed within plagioclase. Brittle deformation was interpreted from intragranular fractures. Crystal plastic deformation was interpreted from undulose extinction, bulged grain boundaries, kinked twins, and subgrain boundaries. Crystal plastic recovery was interpreted from recrystallized grains around plagioclase edges. Alteration was evidenced by partial to near complete sericitization of plagioclase grains.

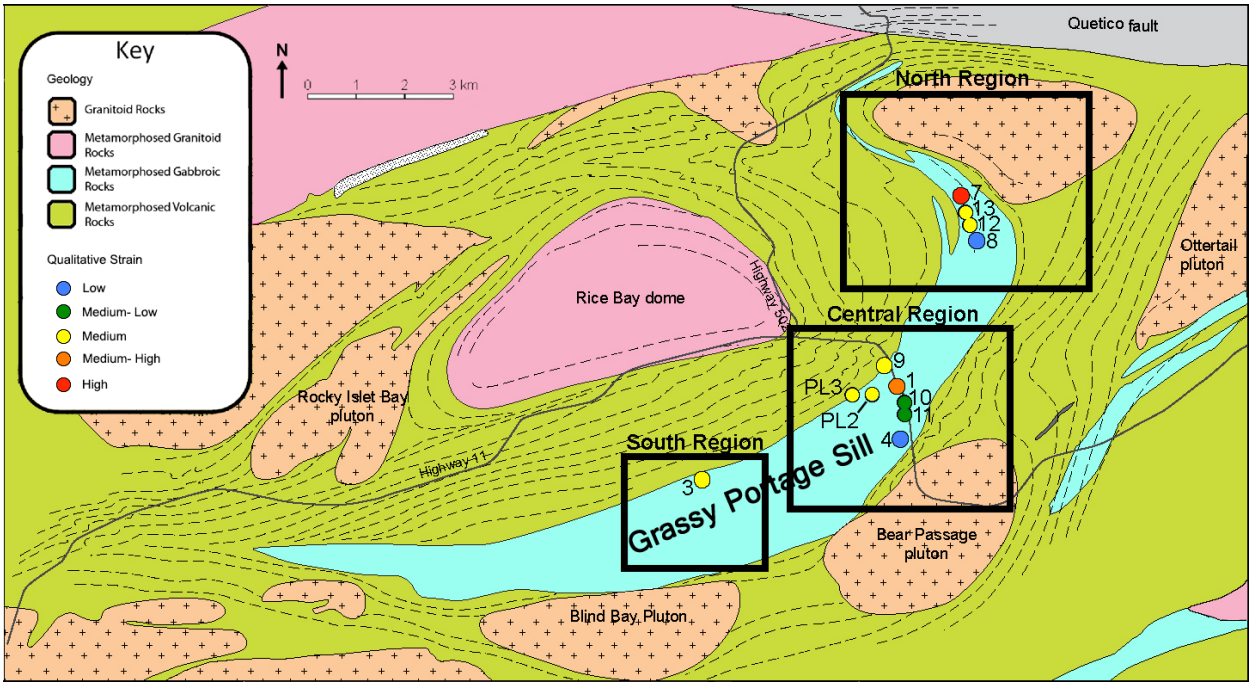

Figure 7. Simplified geologic map with the three main outcrop bearing regions. Outcrops are color coded based on qualitative strain. Modified from Poulsen (2000) and Druguet et al. (2008).

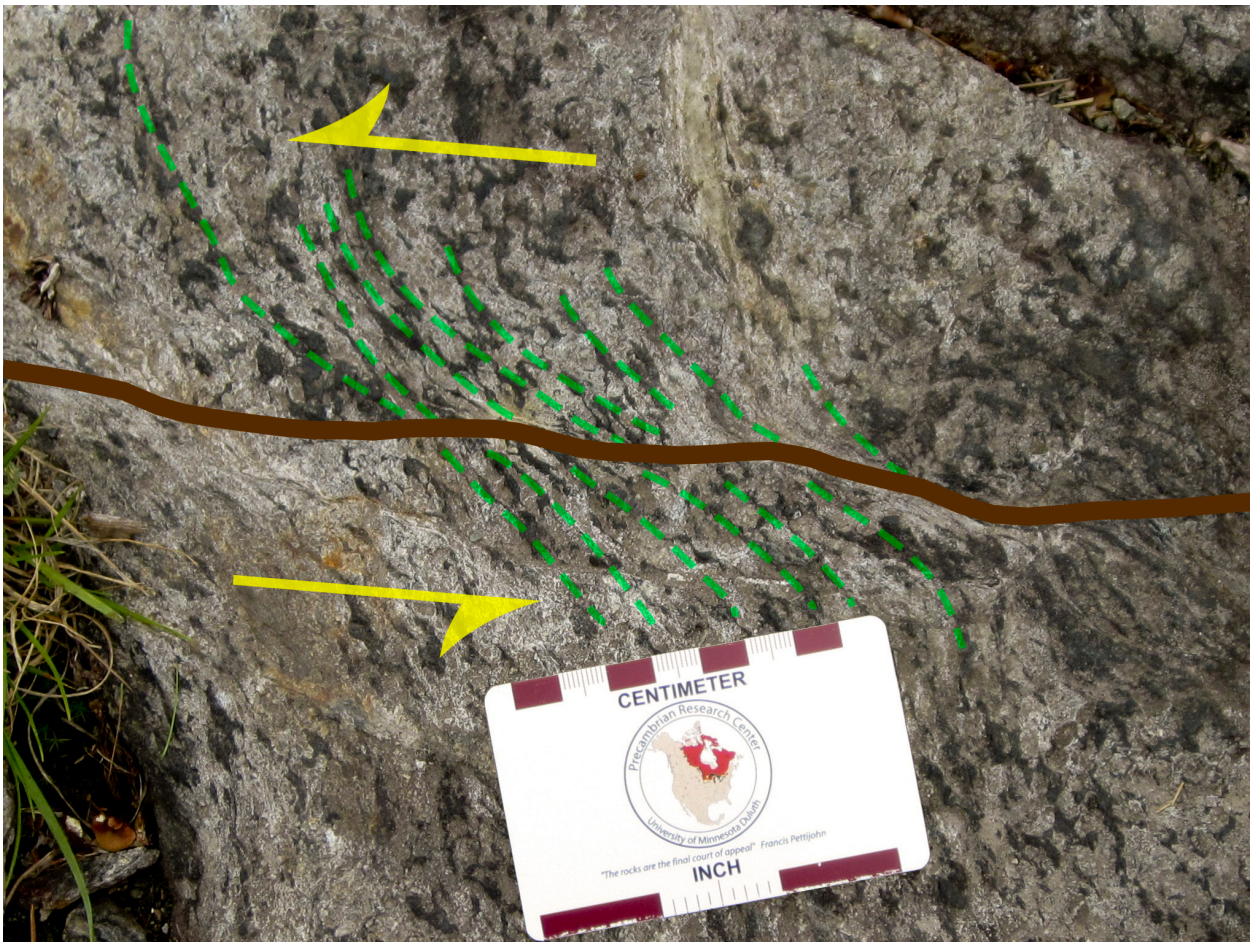

Figure 8. Subhorizontal photograph at GPS11-01 outcrop showing fabric deflection in a sinistral shear zone. Brown line is shear zone trace and green dashed lines indicate foliation deflection. Location shown on Fig. 7.

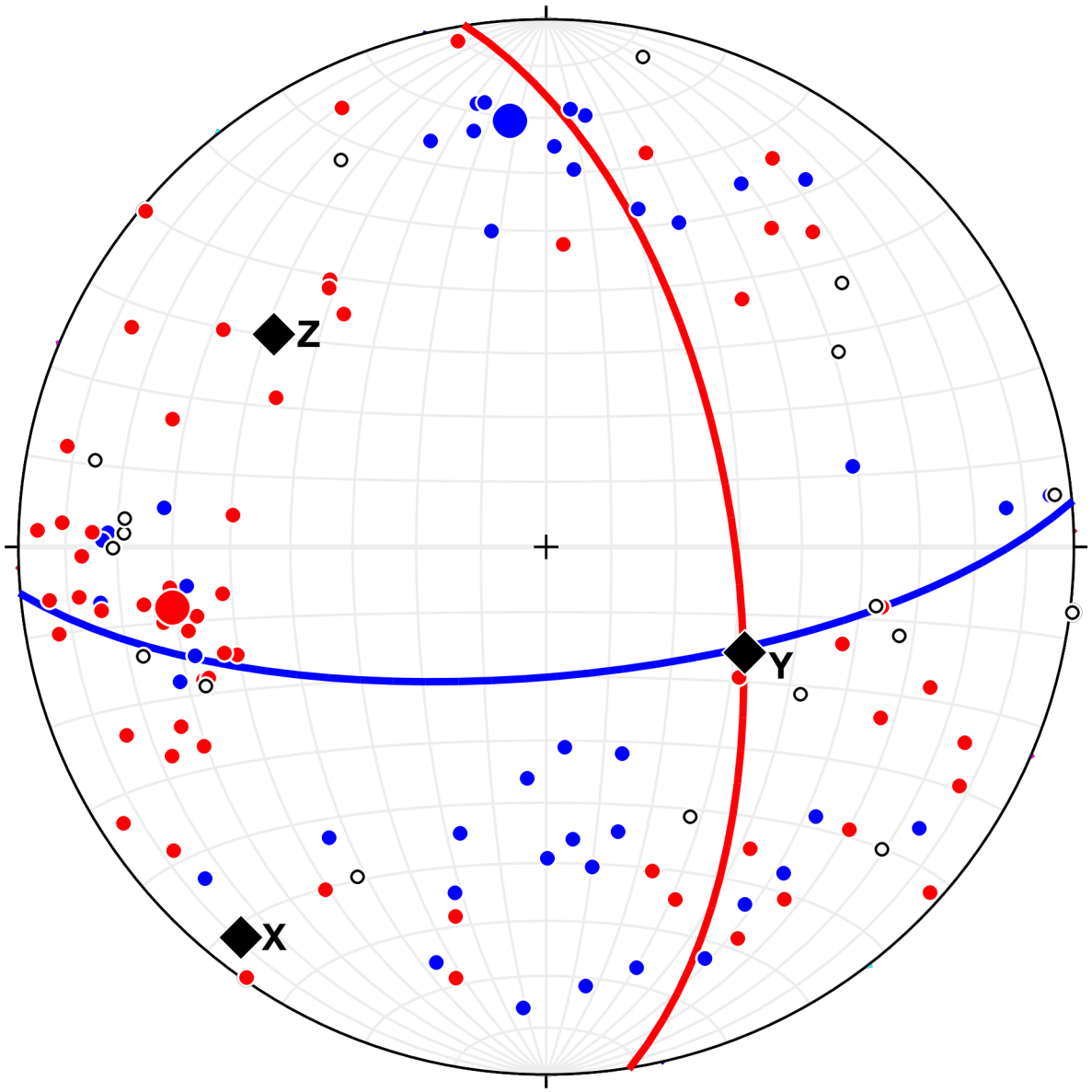

Figure 9. Example of a Stereographic Projection plot used in field data analysis. Small dots are poles to shear zone planes (blue for dextral, red for sinistral, hollow for uncertain shear sense). Great circles and large dots indicate mean vector of pole, and corresponding planes. Diamonds indicate bulk finite stretching axes (X, Y, and Z).

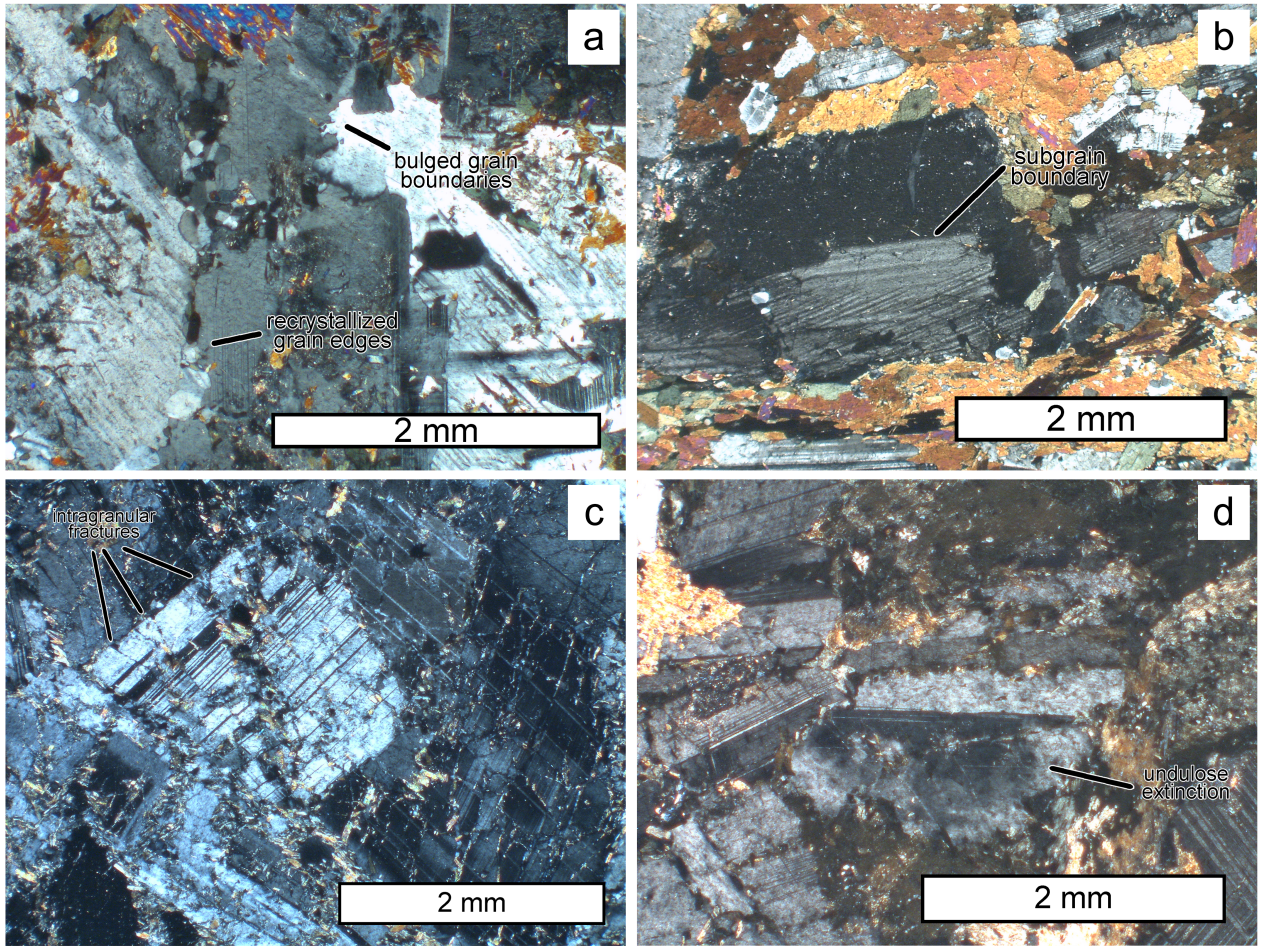

Figure 10. Photomicrographs displaying variation in microstructures observed in plagioclase. **(a)** Bulged grain boundaries and recrystallized edges from GPS11-07a XY plane. **(b)** Subgrain boundary from GPS11-08a XY plane. **(c)** intragranular fractures from GPS11-01b XY plane **(d)** Undulose extinction from GPS11-03b XY plane.

Chapter 4: Results

4.1 Field Results.

4.1.1 Outcrop Descriptions

Within the GPS, the accessible outcrops were found within three distinct and accessible regions (Fig. 7). The north region is a series of logging roads, the central region is a series of roadway exposures along Highway 11 in addition to two outcrops exposed by a power line traverse, and the south region is a previous mining operation site. Where given, strike and dip measurements use right-hand-rule convention (strike/dip) and lineations are given as plunge/trend.

4.1.1.1 North Region

GPS11-07:

This outcrop is composed of four approximately 2-meter by 1-meter subhorizontal exposures, which were hand cleared for this work. GPS11-07 is the northernmost within the north region, the gabbros are coarse grained (>1cm), and primarily composed of plagioclase surrounding larger grains of hornblende, with minor amounts of biotite and chlorite. Semi-ellipsoidal anorthositic pods are contained in the gabbros. This outcrop had a weak foliation oriented 316/90.

GPS11-07 contains 36 shear zones, comprised of twelve dextral, fifteen sinistral and nine of ambiguous sense of motion. The average strike of dextral sets is 154°, while the sinistral sets have an average strike of 103°. Shear zones range in thickness up to 5 cm, with shear zones often localizing at the boundary between gabbro and anorthositic pods. There was mutual crosscutting of dextral and sinistral shear zones, with neither being dominant throughout the outcrop.

GPS11-13:

GPS11-13 is a sub-horizontal exposure with five shear zones comprised of three dextral, one sinistral and one of ambiguous sense of motion, located south of GPS11-07. The dextral shear zones have an average strike of 142°, while the sinistral average 059°. It contains a contact between coarse grained (>1cm) and medium-grained (<1cm) gabbro, both of which are primarily composed of plagioclase and hornblende with minor amounts of biotite.

Most of the outcrop contains coarse-grained gabbro in which large hornblende megacrysts (approximately 1-3 cm) are surrounded by finer plagioclase. There are a variety of shear zones up to 3cm thick, and multiple elongated anorthositic pods. A smaller portion of the outcrop contains medium-grained gabbros, which are mostly composed of equal amounts of plagioclase and hornblende with grain size of <1cm.

GPS11-12:

This is a subhorizontal exposure with a total of eight shear zones comprised of three dextral and five sinistral, located south of GPS11-13. The mineralogy is primarily composed of plagioclase and hornblende with minor biotite and chlorite. This outcrop does not contain any anorthositic pods.

Within this outcrop there are both shear zones and a strong foliation. The shear zones are oriented in two dominant directions with dextral striking 172° and sinistral striking 085° on average. The rocks surrounding the shear zones contain a strong foliation oriented approximately 122/75, and a lineation of 06/126.

GPS11-08:

GPS11-08 is the southernmost outcrop within the north region. It has a total of three shear zones comprised of two dextral and one sinistral. The mineralogy is the same as the other

sites within the north, primarily plagioclase and hornblende, with minor biotite and chlorite. This site has significantly finer grain size (<1mm) than the rest of the region. In addition to shear zones, this outcrop had a strong foliation oriented 118/60.

The entire outcrop has a very strong pervasive foliation. This outcrop has significantly fewer shear zones, measured in both quantity and density. The shear zones that are present are very thin (<0.5cm). Quartz veins were offset by shear zones.

4.1.1.2 Central Region

GPS11-09:

GPS11-09 contains a total of 42 shear zones comprised of eleven dextral, 24 sinistral and seven of ambiguous sense of motion. It is located near the western boundary of the sill, composed of surficial roadside outcrops and an adjacent exposure created by a railroad line which runs beneath Route 11. It contains coarse-grained (>1cm) gabbros. Plagioclase is the dominant mineral, with hornblende as the secondary, and minor amounts of both biotite and chlorite. This outcrop had a weak foliation that is oriented 026/87.

This outcrop contains a moderate quantity of shear zones, ranging in thickness from <0.5cm up to 2.5cm. The dextral shear zones have an average strike of 131°, while the sinistral have an average strike of 151°. There is no apparent foliation or anorthositic pods.

GPS11-01:

GPS11-01 is a road outcrop with a total of 62 shear zones comprised of eighteen dextral, 37 sinistral and seven of ambiguous sense of motion. The exposure straddles both sides of Highway 11, south of GPS11-09. Coarse-grained (>1cm) gabbros of various compositions interfinger with metavolcanics. Gabbro is composed primarily of plagioclase and hornblende, varying from

plagioclase-dominant to subequal plagioclase and hornblende, with minor quantities of biotite and chlorite throughout. Garnet is visible at the contacts between gabbro and metavolcanics.

Shear zones, up to 2 cm thick, are prevalent throughout the outcrop. Grain size reduction is apparent within the shear zones. The dextral shear zones have an average strike of 107°, while the sinistral shear zones have an average strike of 032°. The 35 anorthositic pods in the outcrop showed signs of deformation, having an average sub-horizontal aspect ratio of 2.1 and an overall oblate shape.

GPS11-10:

GPS11-10 is comprised of 8 shear zones with three dextral, five sinistral and one of ambiguous sense of motion. It is located south of GPS11-01 along Highway 11, along both sides of the highway. The dextral shear zones have an average strike of 084°, while sinistral shear zones have an average strike of 056°. Gabbros are coarse-grained (>1cm), primarily composed of plagioclase and hornblende, with secondary biotite and chlorite and visible ore mineralization.

Shear zones here are less dense than at outcrops north on the Highway 11 traverse. In addition to shear zones, there are joints, which crosscut shear zones. Where observed, shear zones are relatively thin, up to 0.5cm.

GPS11-11:

GPS11-11 is located south of GPS11-10 on Highway 11. It contains ten total shear zones, with one dextral, eight sinistral, and one of ambiguous sense of motion. Dextral shear zones have an average strike of 086°, while sinistral average 167°. Gabbros are coarse-grained and compositions vary. Some are predominantly composed of plagioclase and hornblende and host shear zones, whereas some have a greater percentage of plagioclase with trace garnet up to 1 cm in diameter and lack of shear zones. This outcrop has extensive jointing which cross cuts shear

zones, but are less prevalent than GPS11-10, as well as a moderate foliation oriented 252/82, and a lineation of 32/226

GPS11-04:

The southernmost exposure along the Highway 11 north-south traverse, GPS11-04 is located near the eastern boundary of the GPS. The outcrop contains structural variations in the form of a developing foliation and jointing, in addition to interfingering of metasedimentary units. There is a complete lack of shear zones.

The gabbro in the northern part of the exposure is very fine grained, with plagioclase and hornblende interlocking in a sugary texture. There are no obvious foliations or shear zones, and only a few interspersed joints. Southward, fine grain size is maintained, while both a foliation and jointing develop. Foliation has an average orientation of 249/65. Three distinct jointing sets are oriented approximately 352/71, 234/57, & 270/75. Subvertically oriented mica schist interfingers with gabbro at the southern edge of the outcrop.

PL2 & PL3:

PL2 and PL3 are two exposures located along a power line traverse which crosses Hwy 11 at the site of GPS11-01, with PL2 located west of GPS11-01, and PL3 located west of PL2. PL2 has nine shear zones, with six dextral with an average strike of 044°, one sinistral with a strike of 170° and two with ambiguous sense of motion. PL3 has five shear zones, with three dextral, with an average strike of 017°, one sinistral with a strike of 070°, and one with an ambiguous sense of motion.

Both outcrops are coarse grained, primarily composed of plagioclase and hornblende with minor biotite. Shear zones vary in thickness up to 2 cm with a majority being discrete (<0.5 cm). There are a few lenticular anorthositic pods within both exposures, which have an oblate shape.

4.1.1.3 South Region

GPS11-03:

The only outcrop within the south region, GPS11-03 is a historical mining operation, located at the eastern boundary of the GPS. The site has four approximately 50 meter long exposed tracts of outcrop, running parallel to one another in a NW-SE orientation. Gabbro within these tracts varies, with variation from medium (1mm - 1cm) to coarse (>1cm) grained. Mineralogically there is less variation throughout the gabbro, with approximately equal parts plagioclase and hornblende, with minor biotite/chlorite as well as zones of ore mineralization. Within these four exposures, there are multiple intrusions of interfingered mica-schist units.

Within this site, shear zones are seemingly preferentially located within coarser grained portions of gabbro. Some shear zones appeared to be lithologically bound to the boundary with meta-sedimentary units. The majority of shear zones are thin, less than 0.5 cm thick. In total 122 shear zones were measured, 55 dextral had an average strike of 130°, while 58 sinistral had an average strike of 191°, and nine had an ambiguous sense of motion. There is a weak foliation in the medium-grained section of gabbro which is oriented 083/81 and has a lineation which varies in orientation, but averages 19/075.

4.1.2 Inferred Strain Variation

Unfortunately, as in most deformed rocks, strain markers that can be used to quantify strain are largely absent within the GPS. While the anorthosite pods found within the GPS would serve as good markers for strain analysis, they were only found in three of the studied exposures. Where present, the anorthositic pod dimensions were measured on subhorizontal surfaces, as

listed in Table 2. Their ratio of their long to short dimensions were used to estimate two-dimensional strain of the pods, and rank those three outcrops in terms of their relative strain. Due to lack of anorthosite pods or other strain markers throughout the entire GPS, strain was otherwise inferred by a qualitative assessment of various aspects of the shear zones at each site including the quantity, density and overall thickness/appearance of shear zones. The sites were given qualitative rankings of inferred strain from low to high (Table 2). In general, shear zone density and shear zone thickness were deemed to be the most reliable indicators for relative strain ranking.

Qualitatively, within the northern region of the GPS, strain magnitude ranges from the highest strained site in the sill (GPS11-07) to the lowest strained site (GPS11-08). The highest strained sites within this region are in the north and inferred strain progressively decreases southward.

Within the central region of the sill, there is much less inferred strain variation compared to the northern region. Strain varies between low and medium-high. Generally, strain increases across the sill with low strain to the south and med-high strain at GPS11-01, which is approximately centered in the sill. GPS11-09 and GPS11-04 are located at the margins of the sill and each have inferred strain which is much lower than the next closest sites.

In the southern region of the sill, there is only one site, GPS11-03. This site is located on the western margin of the sill, and has medium inferred strain. This is comparable, in strain magnitude alone, to site GPS11-09, which is also located on the western margin of the sill, although it is located over 2.5 kilometers away in the central region.

Generally, strain patterns were linked to a combination of grain size and inferred bulk strain magnitude. At sites with the finest grain sizes, GPS11-04 and GPS11-08, shear zones are

lacking, and deformation generated a pervasive foliation (Fig. 6). Within other sites, shear zones are prevalent in coarser grained portions of the GPS. Within sites with grain size variations, such as GPS11-03 where grain size varies from medium to coarse grained, shear zones were preferentially found within the coarse-grained portions. Additionally, some sites had fine grain size (GPS11-11; Table 2), but had relatively well developed shear zones. This site had shear zones up to 1.5 cm in thickness, which indicated that despite a fine grain size, a high strain magnitude at the site caused the development of shear zones.

4.1.3 Foliation

Throughout the Grassy Portage Sill, foliation was observed within seven of the twelve studied outcrops (Fig. 11). When present, foliation was defined by the alignment of hornblende. Foliation was significantly more prominent and pervasive in finer grained sections of the GPS, and was accompanied by a lack of shear zone density.

Foliation orientation varied similarly to the surrounding rock units (Fig. 11). In the north, the three outcrops with foliations have an average strike of 305°/125°. In the central portion of the sill, the three outcrops with foliation had an average strike of 058°/238°. In the southernmost outcrop, the foliation found at the only measured outcrop, strikes 083°/263°. This variation in foliation is similar to the regional foliation, which appears to deflect around the Rice Bay Dome located west of the GPS. From these foliation orientations, we would deduce a NE-SW finite shortening direction within the northern region, and a NW-SE to N-S oriented finite shortening direction within the central and southern regions. These deduced local shortening orientations vary from the regional deformation which formed through north-south shortening paired with dextral shearing, resulting in an overall transpression. Previous authors have hypothesized that

the foliation deflects due to competence contrasts in rock units; the Rice Bay Dome being more competent than all of the surrounding rock types (Carreras et al. 2010).

4.1.4 Lineation

A weak lineation was measured at four of the twelve studied outcrops within the GPS; it was otherwise not present. Lineation, similar to foliation, was defined by the alignment of hornblende. As is generally the case in SL tectonites, which are deformed rocks with both foliation and lineation, lineation orientations were contained on the foliation plane. Throughout all sites with measured lineation, the trend of lineations were approximately parallel to foliation strike, which varied by region (Fig. 12). Lineations plunge shallowly; all plunge <40°, most plunge <30°.

4.1.5 Shear Zones and their Distribution

Shear zones in the GPS were defined by a localized (on the order of mm or cm) deflection and intensification of foliation, specifically of the hornblende, within the GPS. This deflection allowed for the identification of the shear planes, in addition to their sense of motion. Nearly all studied shear zones within the GPS were exposed on the subhorizontal surface. Where three-dimensional exposures of shear zones were available, sense of shear criteria were only observed on the subhorizontal surface.

Of the twelve outcrops investigated, eleven had shear zones in varying quantity and intensity. At these eleven outcrops, a total of 342 shear zones were measured with kinematic shear sense of 137 dextral, 165 sinistral, and 40 ambiguous. Within the northern region, there were a total of 81

measured shear zones, in the central region there were 139 shear zones, and in the southern region there were 122 shear zones.

Where shear zones cross cut, there was mutual cross cutting between dextral and sinistral shear zones. At all outcrops, where crosscutting between shear zones occurred there were examples of both dextral crosscutting sinistral as well sinistral crosscutting dextral.

4.1.6 Synthesis of Shear Zone Field Measurements

To determine the inferred shortening direction and the angle between the strand sets at each site, the measurements were plotted onto stereographic projections, separated by their thickness, and grouped by region (Fig. 13). For thickness, shear zones ≤1cm were categorized as thin, while those >1cm were categorized as thick.

The poles to shear zones for each set were plotted. An average pole orientation was determined to find the average orientation of each set. The angle between the sets can subsequently be determined, which is hypothesized to face the mean shortening direction (Carreras et al., 2010). In Figure 13, these stereographic projections are shown with their spatial location on the sill to compare the variation in both geometry and inferred mean shortening direction throughout the sill.

All sites with shear zones contain strands with both dextral and sinistral sense of motion. Regionally, each set has preferential orientations. In the southern region, dextral strands strike approximately 297°/117°, and sinistral strands strike approximately 029°/209°; in the central region dextral strike approximately 275°/095°, and sinistral strike approximately 197°/017°; and in the northern region dextral strike approximately 156°/336°, and sinistral strike approximately 100°/280°. While all shear zones were steeply dipping, when vertical faces were available they

showed curvature at depth. The networked orientations combined with curvatures results in large shear zone bound lozenges. The obtuse angle between dextral and sinistral sets is interpreted to represent the inferred shortening direction.

For all three regions, the maximum bulk stretching axes were calculated and plotted (X,Y,Z on Fig. 13). For the northern region, the minimum finite strain axis (Z) was 33/040 for the thin shear zones and 38/037 for thick, the intermediate finite strain axis (Y) was 57/212 for thin shear zones and 52/221 for thick shear zones, and the maximum finite strain axis (X) was 05/310 for thin shear zones and 02/128 for thick shear zones. For the central region, the minimum finite strain axis (Z) was 04/314 for the thin shear zones and 11/158 for thick, the intermediate finite strain axis (Y) was 68/052 for thin shear zones and 73/028 for thick shear zones, and the maximum finite strain axis (X) was 22/224 for thin shear zones and 13/248 for thick shear zones. For the southern region, the minimum finite strain axis (Z) was 04/339 for the thin shear zones and 18/164 for thick, the intermediate finite strain axis (Y) was 70/081 for thin shear zones and 67/024 for thick shear zones, and the maximum finite strain axis (X) was 20/250 for thin shear zones and 16/254 for thick shear zones.

Pie charts (Fig. 14) for the three regions help compare the quantities of both dextral and sinistral shear zones. These are separated by both sense of motion (dextral vs. sinistral) and shear zone thickness (thick vs thin).

4.1.7 Shear Zone Thickness Variation

The thickness of each shear zone was measured at the same spot where the orientation was measured. Thin shear zones were defined as those ≤1cm, while thick were those >1cm. The mean, minimum, and maximum width of all shear zones at each site were calculated and plotted

(Fig. 15). Thick shear zones were found within all three regions, at sites GPS11-07 in the north, GPS11-01 in the central, and GPS11-03 in the south.

4.2 Thin Section Analysis

4.2.1 Bulk Mineralogical Composition

Bulk mineralogy was calculated through point counting using a grid of 200 points per thin section. In total, 8 thin sections were analyzed using this method (Fig. 16). The analysis indicates that the Grassy Portage Sill is primarily composed of plagioclase, hornblende and chlorite, with minor amounts of other minerals, indicating gabbro to leucogabbro compositions.

Plagioclase comprised the majority of samples analyzed, ranging from 41% to 69%. The mean average of plagioclase from all samples is 51%. Hornblende ranged from 23% to 37%, and had an average from all samples of 29%. Chlorite was found in 6 of the 8 samples and where present, chlorite ranged from 5% up to 15% with an average of 7%. Other minor minerals present were biotite, quartz, potassium feldspar, calcite, garnet, siderite and clinopyroxene which were found in quantities of less than 5%, in a minority of the samples.

4.2.2 Grain Size Variation in Plagioclase

Grain size was also measured during point counting. Both the long and short grain axes were measured. The long axis measurements were plotted on histograms, separated by site, for analysis (Fig.17-19). To compare across all sites, the same bin sizes were chosen to best display the majority of sites. Plagioclase was the major mineral component and the microstructure-bearing mineral of the Grassy Portage Sill, therefore it was used for the grain size variation analysis. Across the entire GPS, the long axis of plagioclase varied between 0.02 mm and 10.65 mm.

Two samples from the northern region were analyzed for grain size, GPS11-07a and GPS11-08a (Figure 17). In Sample GPS11-07a, representing a high strain site, the majority of grains (54%) were >2mm and ≤ 5mm. In GPS11-08a, which contained very few shear zones, 85% of grains were ≤ 3mm, with 43% ≤1mm.

Within the central region, five samples from four sites were analyzed, GPS11-01b, GPS11-04a, GPS11-11a and two samples from GPS11-09 (Fig. 18). In GPS11-01b, a medium-high strain site, 79% of grains were ≤ 4mm in length; in GPS11-04a, a site which lacked any shear zones, 94% of long axes were ≤ 1 mm; in GPS11-11a, a medium-low strain site, 95% of long axes were ≤ 1 mm; in GPS11-09, a medium strain site, sample A had 85% of axes ≤3mm, while sample B had 94% of axes ≤ 1mm.

In the southern region, one sample was analyzed from site GPS11-03, a medium strain site (Figure 19); 97% of its long axes were ≤ 4mm in length.

Grain size varied significantly at both the outcrop and regional scale, even showing significant variation within a single outcrop. It was noted in the field that the two sites with a lack of shear zones (GPS11-04) or a very low quantity and density of shear zones (GPS11-08) both had very fine (<1mm) grain size. Figure 20, which shows percentage of plagioclase as compared to grain size (long axis length of plagioclase), indicates that there is no apparent relationship between them.

4.2.2 Microstructural Features of Plagioclase

Petrographic analysis of 8 samples, representing 7 sites within the Grassy Portage Sill, indicates that plagioclase serves as the primary microstructure-bearing mineral. The analyzed microstructures have been interpreted to represent a wide range of deformation mechanisms,

which include brittle, crystal plastic and recovery mechanisms, as well as some alteration structures (Fig. 21).

The northern region is represented by two samples, GPS11-08aXY (low strain) and GPS11-07aXY (high strain). Both samples displayed minor amounts of intragranular fracture, significant undulose extinction, bulged grain boundaries, subgrain boundaries and recrystallized edges, in addition to extensive partial sericitization and minor alteration. This microstructural combination would indicate minor brittle deformation, with predominant crystal plastic deformation and subsequent recovery, and finally minor to moderate alteration.

The central region is represented by five samples from four sites: GPS11-04aXY (low strain), GPS11-11aXY (medium-low strain), GPS11-09aX and GPS11-09bXY (medium strain), and GPS11-01bXY (medium-high strain). Plagioclase grains within two sites contain significant intragranular fractures, which indicate brittle deformation: med-high strain for 01b (86%) and medium for 09a (32%), while the rest of sites all have <2% of grains exhibiting it. In contrast, within sample 04a, nearly every plagioclase grain exhibited undulose extinction (99%), as compared to <20% occurrence in the other four samples indicating more crystal-plastic deformation. Bulged grain boundaries were observed in more than half of all grains. Sub-grain boundaries and recrystallized edges, while both found in all four samples, showed no observable trends in occurrence.

The southern region is represented by a sample from one site, GPS11-03bXY (medium strain). It shows a greater occurrence of brittle deformation interpreted structures as compared to the rest of the GPS. Within crystal plastic inferred structures, 03b shows undulose extinction and bulged grain boundaries on par with the rest of the sill, but significantly lesser sub-grain

boundaries as compared to sites within the rest of the GPS. In addition this southern site lacks any grains with recrystallized edges, indicating lack of recovery.

Generally, crystal plastic is the dominant deformation mechanism throughout the three regions, as evidenced by the extensive and dominant bulged grain boundaries, subgrain boundaries, and recrystallization at grain boundaries. In the northern region both deformation and subsequent recovery are prominent whereas in the central and south it appears that dislocations were able to proceed with lesser amounts of recovery.

GPS11-01 Medium-High Strain			GPS11-07 High Strain			Carreras et al. 2010 site High Strain		
Long Axis	Short Axis	L/S Ratio	Long Axis	Short Axis	L/S Ratio	Long Axis	Short Axis	L/S Ratio
16.3	9.4	**1.7**	4.8	1.9	**2.5**	13.7	5.4	**2.5**
27	9.1	**3.0**	6.1	2.9	**2.1**	47.6	14	**3.4**
38.2	7.6	**5.0**	4.6	3.2	**1.4**	7.6	2.9	**2.6**
10.1	7.2	**1.4**	2	1.5	**1.3**	44.9	8	**5.6**
33.3	7.1	**4.7**	2.6	1.4	**1.9**	7.6	3.4	**2.2**
20.6	5.3	**3.9**	3.9	2.4	**1.6**	6.7	3.2	**2.1**
4.2	2.5	**1.7**	2.7	1.6	**1.7**	11.6	6.2	**1.9**
7.4	4.8	**1.5**	4	3.2	**1.3**	10.2	6.9	**1.5**
4	1.9	**2.1**	3.3	2	**1.7**	7.3	2.4	**3.0**
11.7	3.2	**3.7**	12.2	5.3	**2.3**	4.6	1.9	**2.4**
4.6	3.2	**1.4**	11.4	4.6	**2.5**	19.2	7.3	**2.6**
4.7	3.9	**1.2**	11	4.2	**2.6**	9.3	4.2	**2.2**
19	7.9	**2.4**	4.6	2.3	**2.0**	12.1	5.5	**2.2**
3.5	3.5	**1.0**	11.3	4.4	**2.6**	43.2	3.6	**12.0**
5.8	3.2	**1.8**	7.6	1.6	**4.8**	41	9.9	**4.1**
9.1	7.4	**1.2**	6.7	4.5	**1.5**	11.4	4.5	**2.5**
9.9	5	**2.0**	7.9	3.6	**2.2**	7	2	**3.5**
17.4	10.5	**1.7**	13.3	4.6	**2.9**	14.8	4.4	**3.4**
14.3	9.6	**1.5**	12	4.1	**2.9**	7.6	4.4	**1.7**
12.6	6.4	**2.0**	8.6	4	**2.2**	7	2.4	**2.9**
5.1	1.8	**2.8**	10.2	3.8	**2.7**	62.5	9.5	**6.6**
4.6	3.5	**1.3**	9.2	2.9	**3.2**	33	10.9	**3.0**
8.1	6.3	**1.3**	4.6	2.1	**2.2**	43.6	12.7	**3.4**
7.3	6.1	**1.2**	13.9	5.1	**2.7**	16.4	7.6	**2.2**
9.5	4	**2.4**	9.3	6	**1.6**	33.6	11.4	**2.9**
8.8	5.6	**1.6**	7.2	2.7	**2.7**	41.4	9.4	**4.4**
26.2	13.8	**1.9**	11.1	6.9	**1.6**	76	8	**9.5**
11.4	8.7	**1.3**	5.2	3.4	**1.5**	14.6	4.5	**3.2**
9.6	6.4	**1.5**	3.6	2.5	**1.4**	51	15.4	**3.3**
5.4	4.1	**1.3**	12.4	7.1	**1.7**	37.6	9.4	**4.0**
11	7.3	**1.5**	4.5	3.2	**1.4**	24	12.2	**2.0**
			6	4.1	**1.5**	25.7	9.6	**2.7**
			6.7	2.6	**2.6**	14	8.3	**1.7**
			5.1	3.3	**1.5**	24.6	8.7	**2.8**
			6.1	3.6	**1.7**	19	14	**1.4**
						22.4	14.5	**1.5**
						41.4	15.1	**2.7**
						15.3	9.2	**1.7**
						18.5	10.6	**1.7**
						12.4	5.6	**2.2**

Site	GPS11-01	GPS11-07	Carreras
Average Ratio	2.0	2.1	3.2
Maximum Ratio	5.0	4.8	12.0
Median Ratio	1.7	2.0	2.7

Table 1. Anorthosite data from throughout GPS where present. Long to short ratio of lengths used as strain marker, with ratio of 1.0 assumed to represent pre-deformation geometry of anorthosites. Data was collected at two exposures within GPS in addition to high strain site studied in Carreras et al. 2010, which is located adjacent to GPS11-07.

Grassy Portage Sill Strain								
Site ID	**zone**	**rock type**	**anorthosite blobs**	**foliation intensity**	**shear zone density**	**maximum shear zone thickness (cm)**	**average grain size (mm2)**	**strain ranking**
GPS11-04	Central	Fine Grained Gabbro	None	Strong, Pervasive	None	n/a	0.2	Low
GPS11-08	North	Fine Grained Gabbro	None	Strong, Pervasive	Very Low	0.5	3.8	Low
GPS 11-11	Central	Coarse Grained Gabbro	None	Moderate	Low	1.5	0.6	Medium-Low
GPS 11-10	Central	Coarse Grained Gabbro	None	N/A	Low	1	n/a	Medium-Low
GPS 11-12	North	Coarse Grained Gabbro	None	Strong	Moderate	0.5	n/a	Medium
GPS 11-13	North	Medium to Coarse Gabbro	Slightly Flattened	N/A	Moderate	2.5	n/a	Medium
GPS 11-03	South	Medium to Coarse Gabbro	None	Weak In Fine Grain Portions	Moderate	2	5.5	Medium
GPS 11-09	Central	Coarse Grained Gabbro	None	Weak	Moderate	2.5	3.7	Medium
GPS 11-01	Central	Coarse Grained Gabbro	2.0 Ratio	N/A	High	4	15.2	Medium-High
GPS 11-07	North	Coarse Grained Gabbro	2.1 Ratio	Weak	High	5	35.7	High

Table 2. Table indicating criteria used to determine overall strain rankings of GPS exposures. Where possible, anorthosite blob two-dimensional inferred strain ratios were used for rankings. In most outcrops where these were not present, shear zone density and shear zone thickness were used.

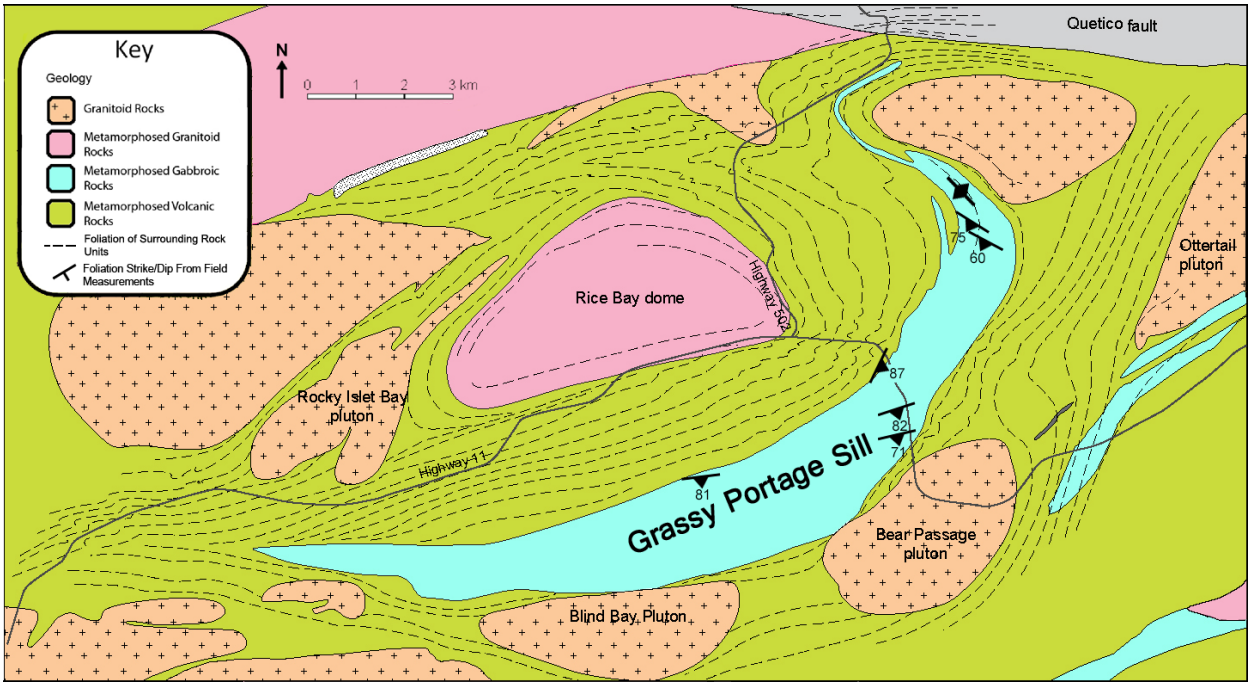

Figure 11. Generalized geologic map (based on Druguet et al., 2008) and foliation measurements of outcrops where rock fabric was apparent. Dashed lines in neighboring units are generalized foliation trajectories from Druguet et al., 2008. Foliation measured in GPS varies along the length of the sill, and similarly to surrounding units, wraps around the Rice Bay Dome.

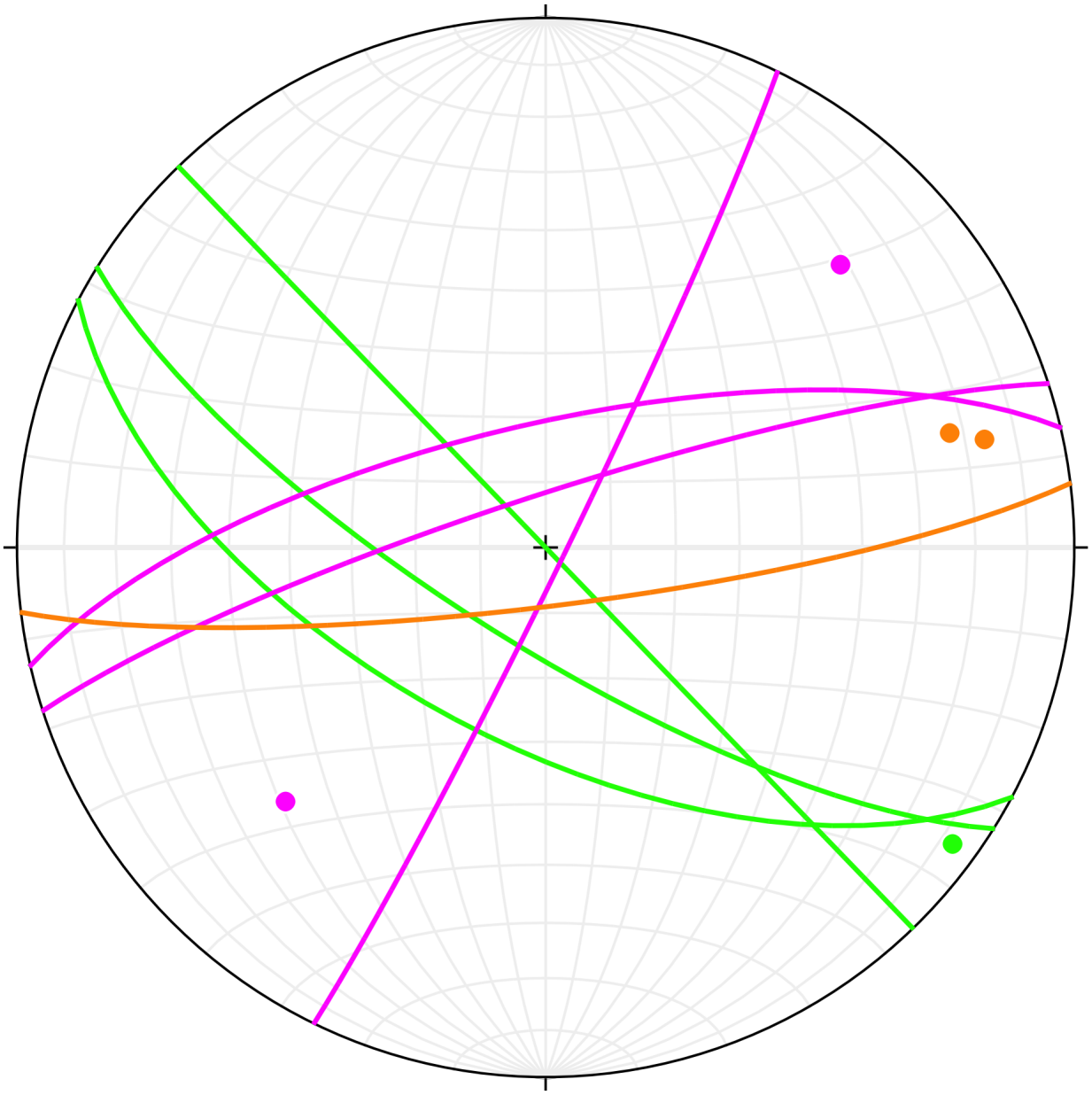

Figure 12. Stereographic projection showing foliation (planes) and lineations (points) throughout GPS. Northern region measurements in green, central region in pink, and southern region in orange.

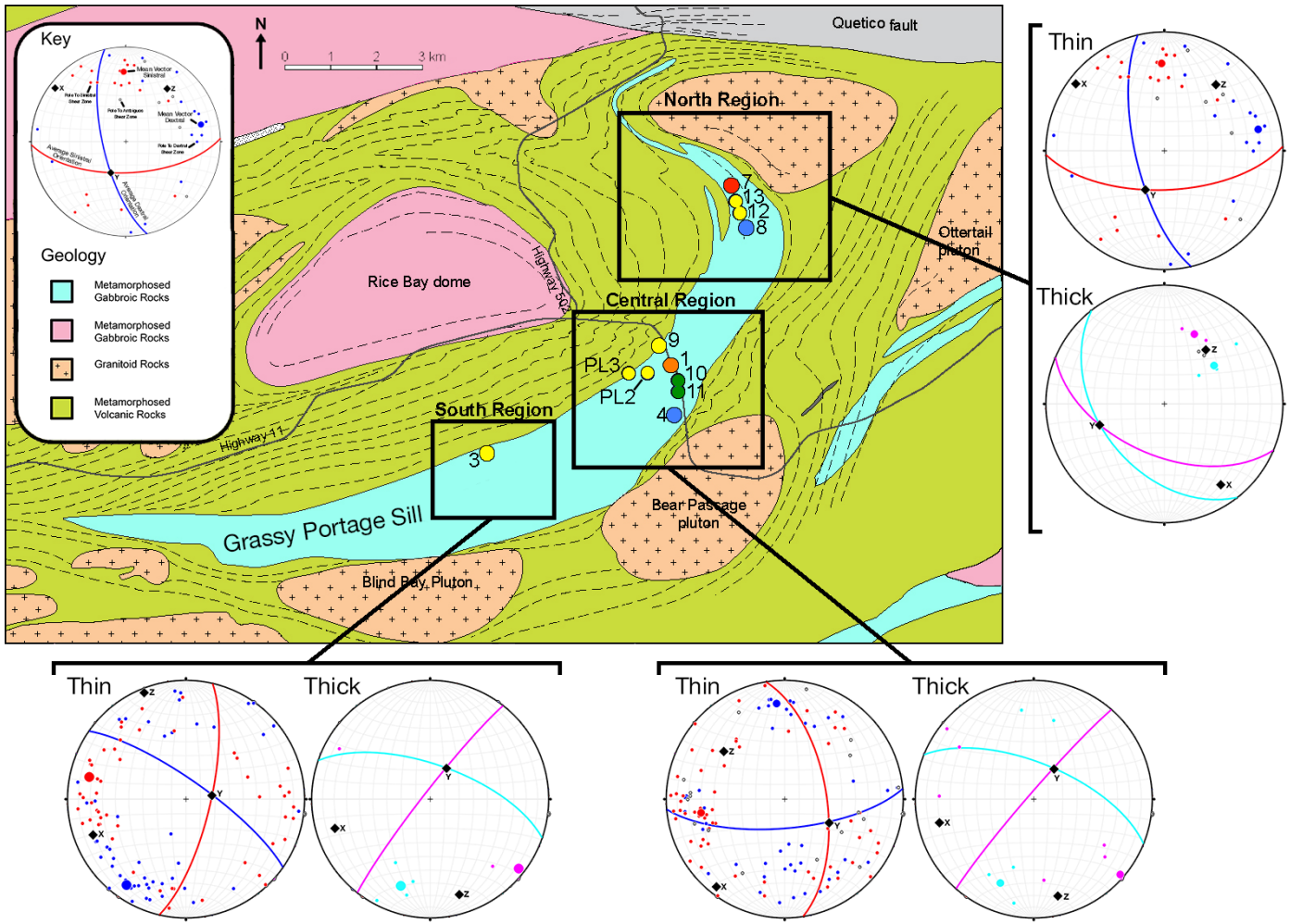

Figure 13. Generalized geologic map of the Grassy Portage Sill and surrounding region, with regional stereographic projections. On stereographic projections, small dots are poles to shear zone planes (blue for dextral, red for sinistral, hollow for uncertain shear sense). Great circles and large dots indicate mean vector of pole and corresponding planes. Diamonds indicate bulk finite stretching axes (X, Y, and Z). Where thick (≥1 cm) shear zones were present, they are plotted separately. Modified from Druguet et al., 2008.

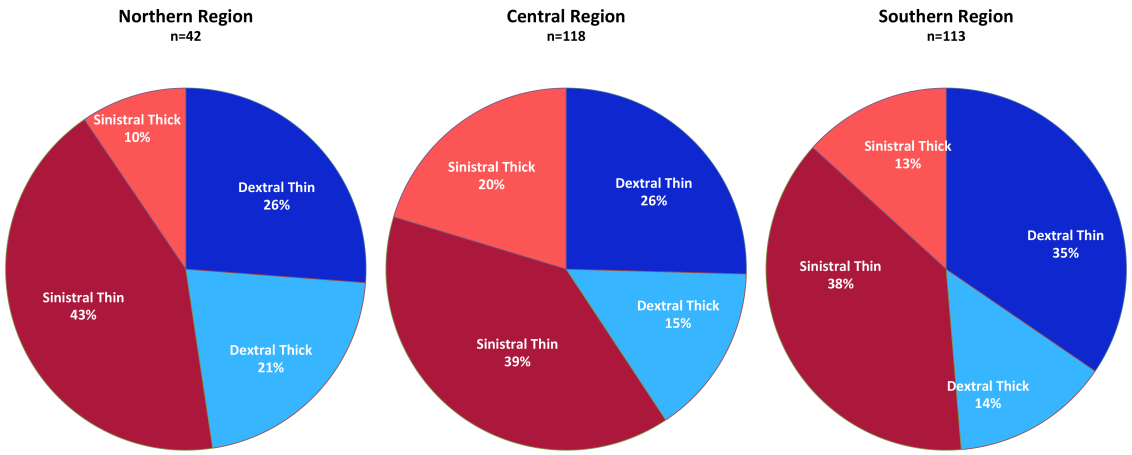

Figure 14. Pie charts indicating percentage of shear zones of dextral and sinistral shear sense within each of the three major regions of the GPS, with approximate 1:1 ratio of total dextral and sinistral shear zones.

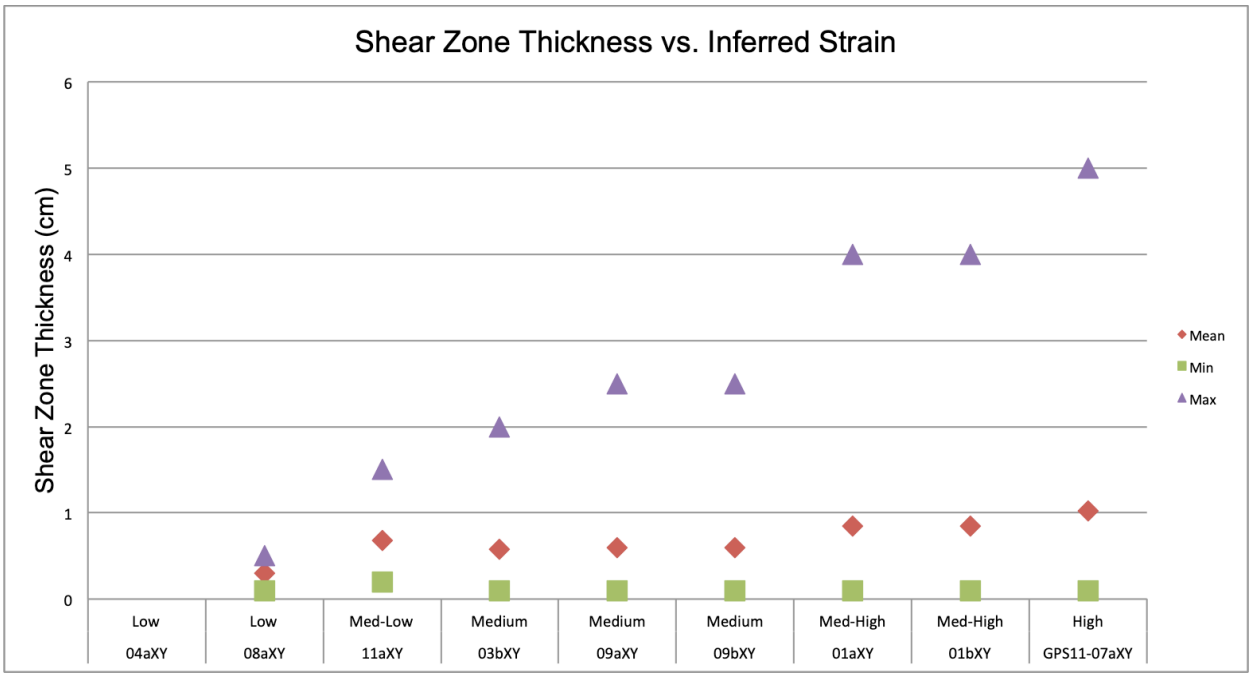

Figure 15. Shear zone thickness variation, separated by site. Sites are ordered from qualitative lowest strain on the left to the highest strain on right. Maximum shear zone thickness at each exposure shows increase with higher deformation.

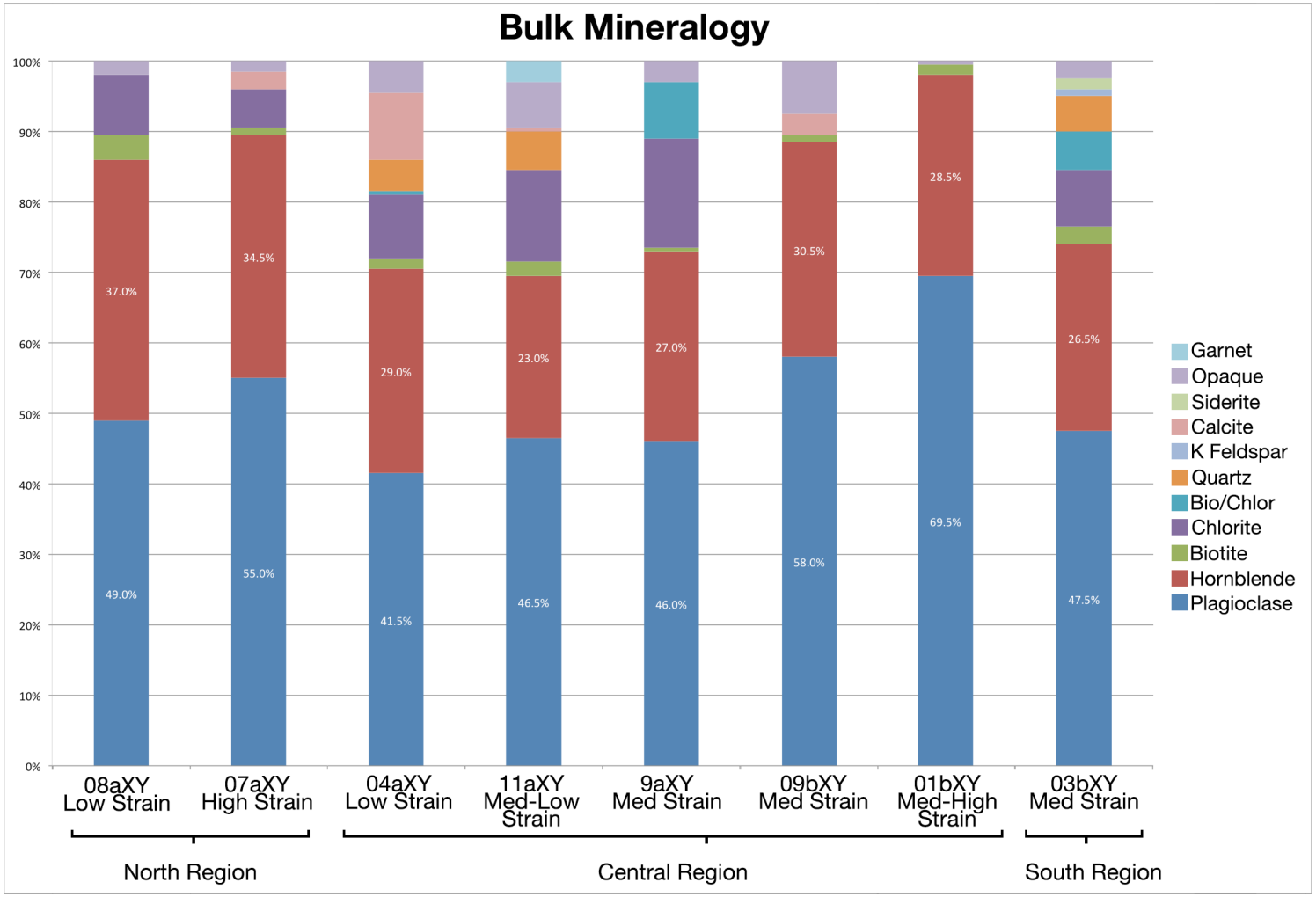

Figure 16. Bulk mineralogy as determined from point counting of the XY plane thin section, grouped by region within field area, and ordered by qualitative strain within each region. Results indicate that mineralogy is largely constant throughout the GPS.

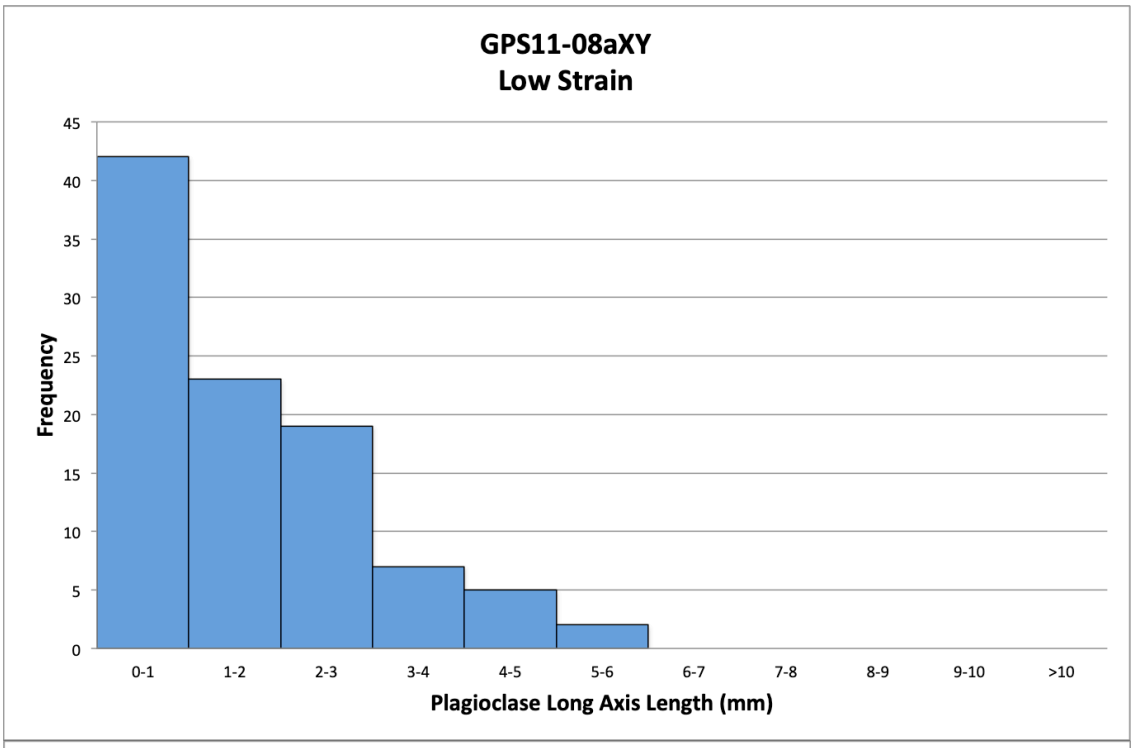

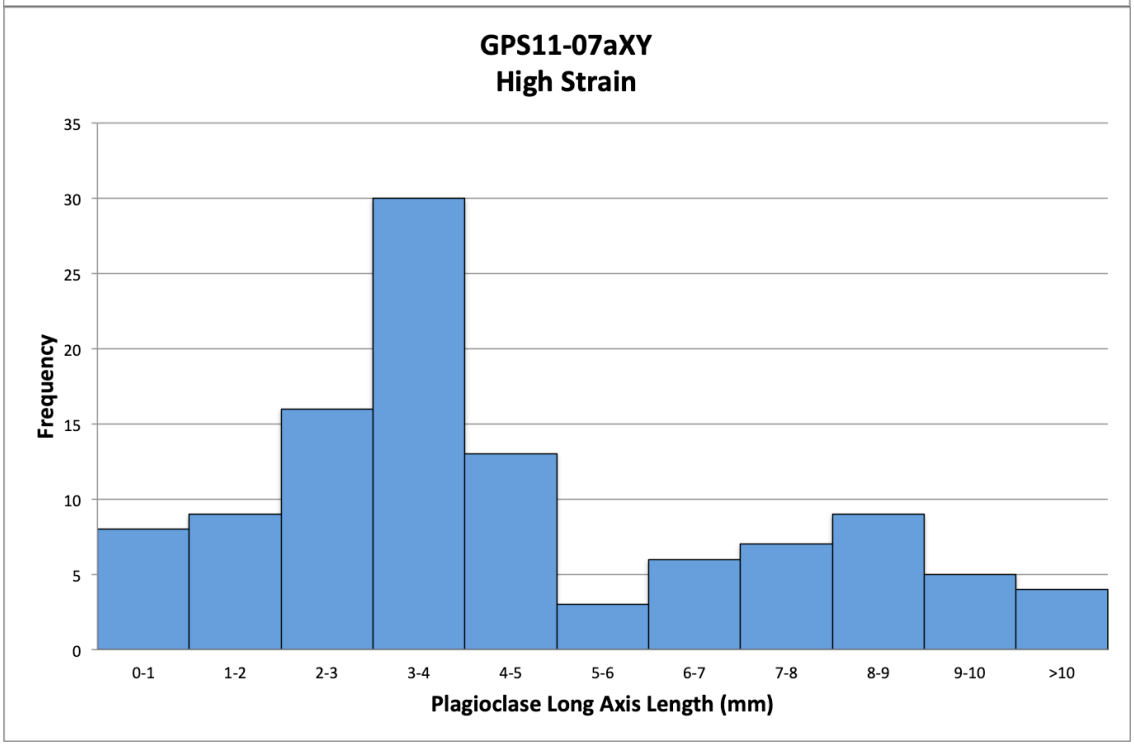

Figure 17. Histograms for grain size (long axis) of plagioclase from sites in northern region of the Grassy Portage Sill. Majority of grains have consistently short axis length, indicating overall fine grain size. GPS11-07 shows a bimodal distribution indicating two distinct grain sizes, one fine and one coarser.

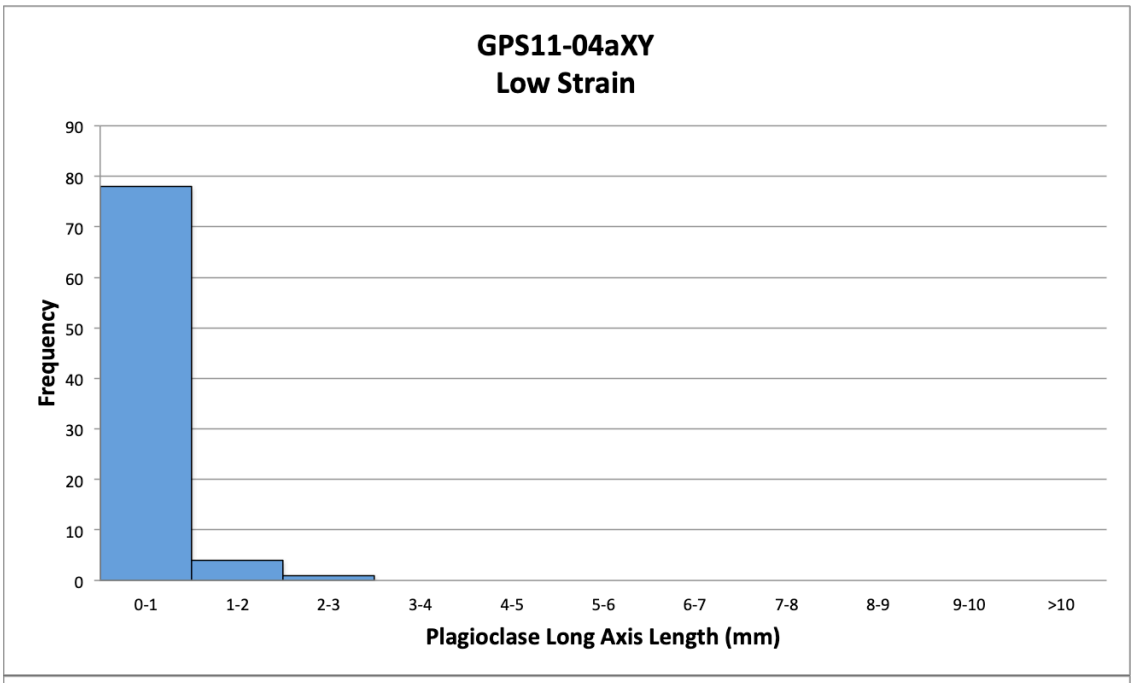

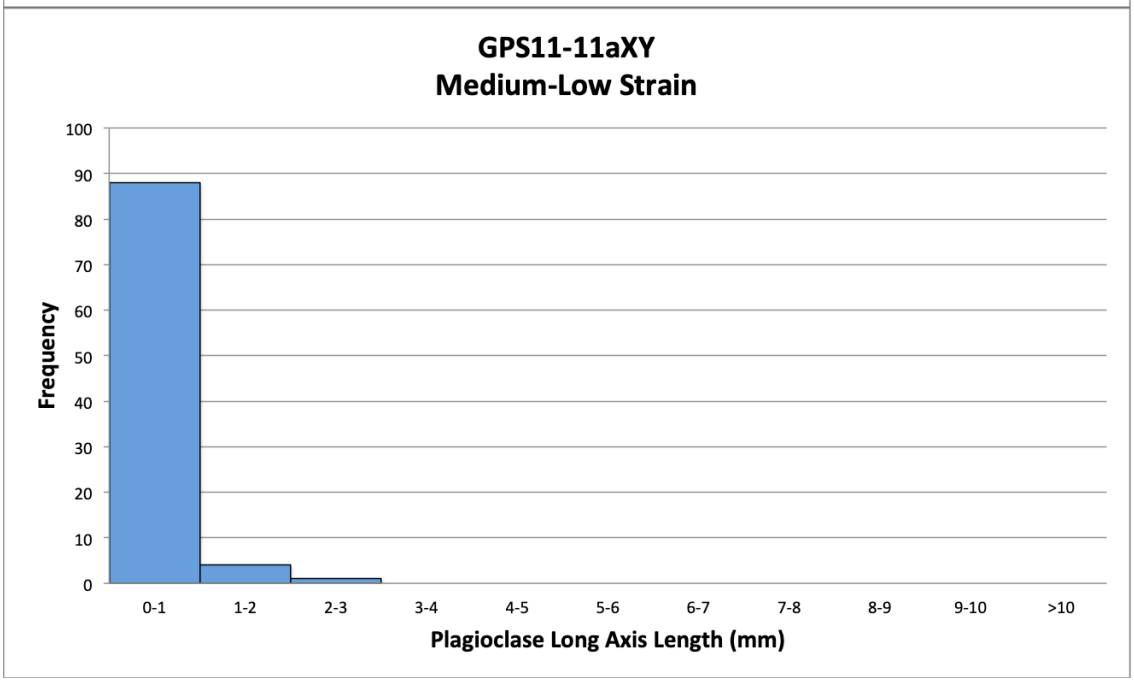

Figure 17. continued

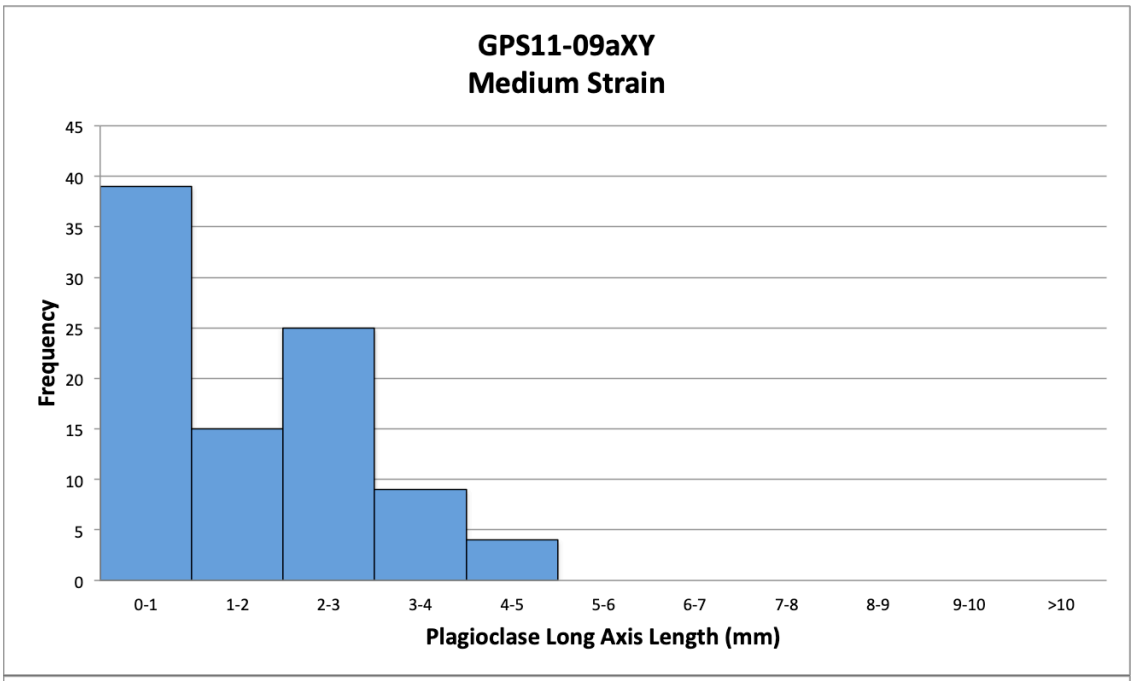

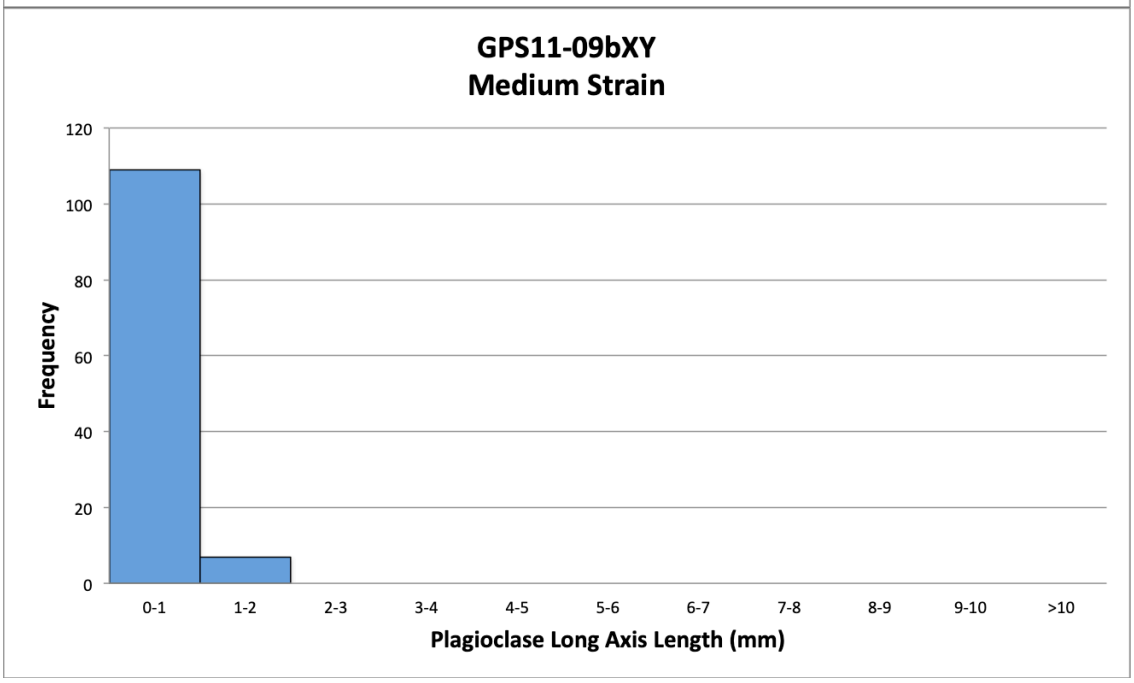

Figure 17. continued

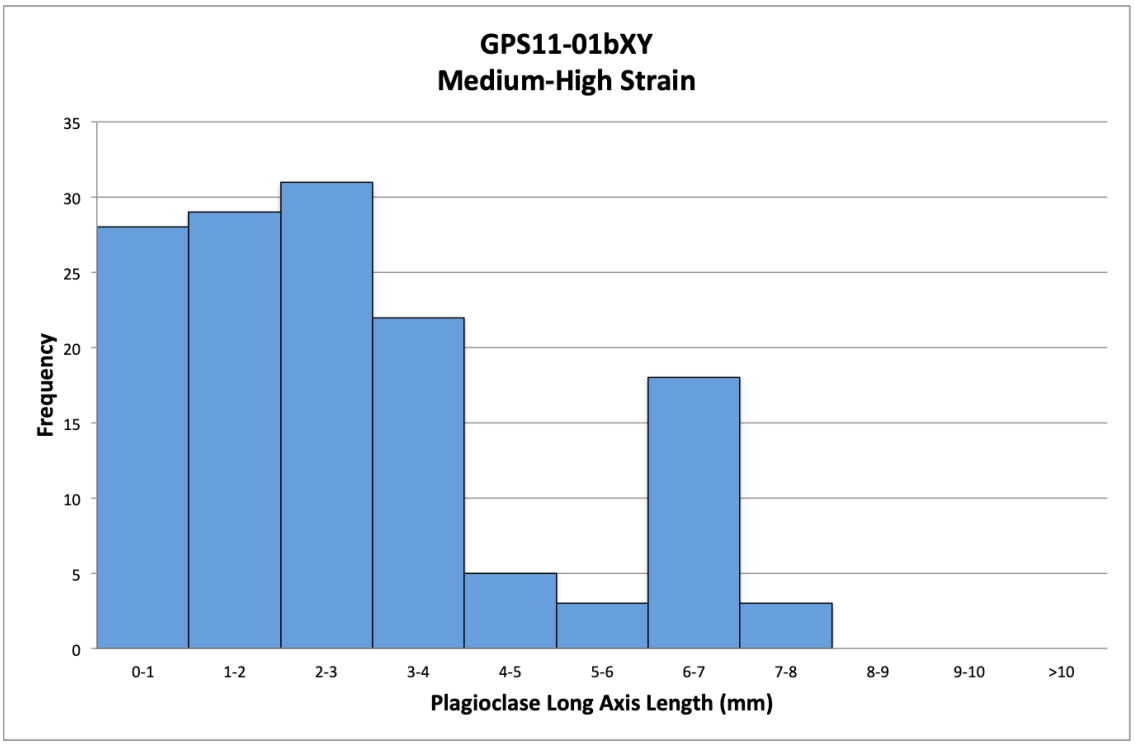

Figure 18. Histograms for plagioclase grain size (long axis) from sites in central region of the Grassy Portage Sill. Majority of grains have consistently short axis length, indicating overall fine grain size, with a second small population of 6-7mm long axis grains, indicating an unequal bi-modal grain size distribution.

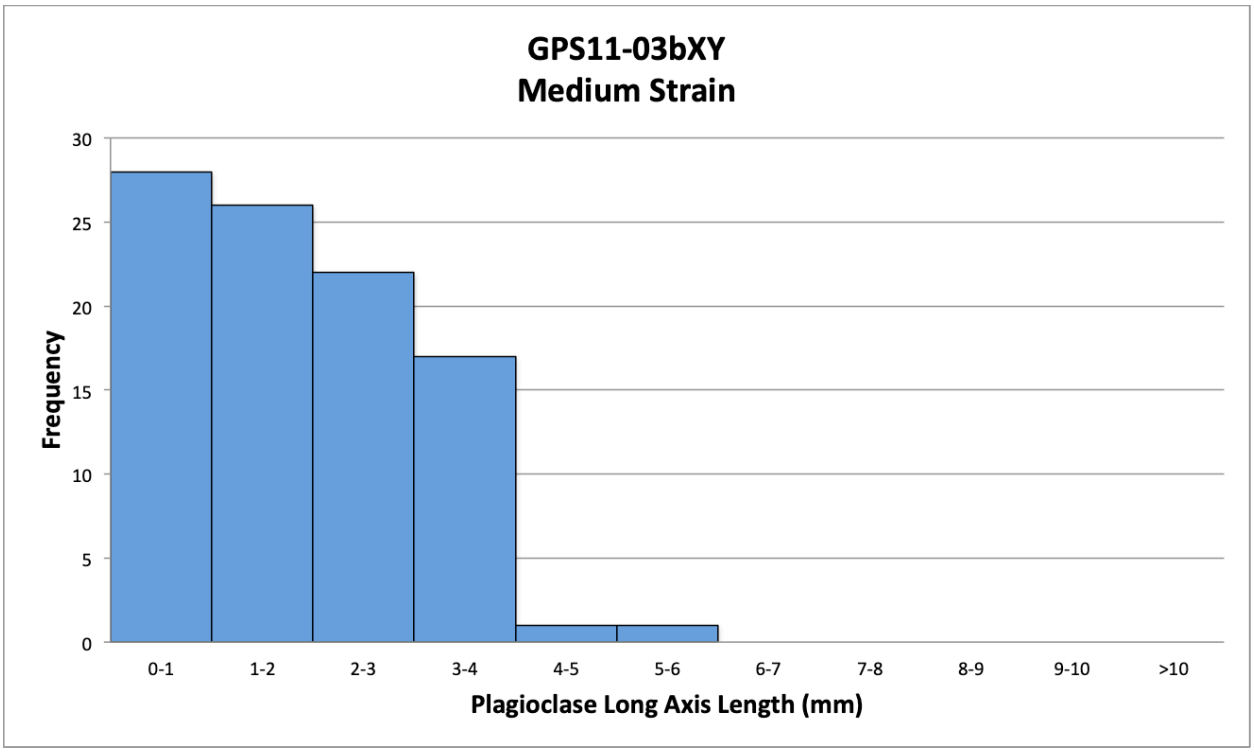

Figure 19. Histograms for plagioclase grain size (long axis) from sites in south region of the Grassy Portage Sill. Majority of grains have consistently short axis length, indicating overall fine grain size.

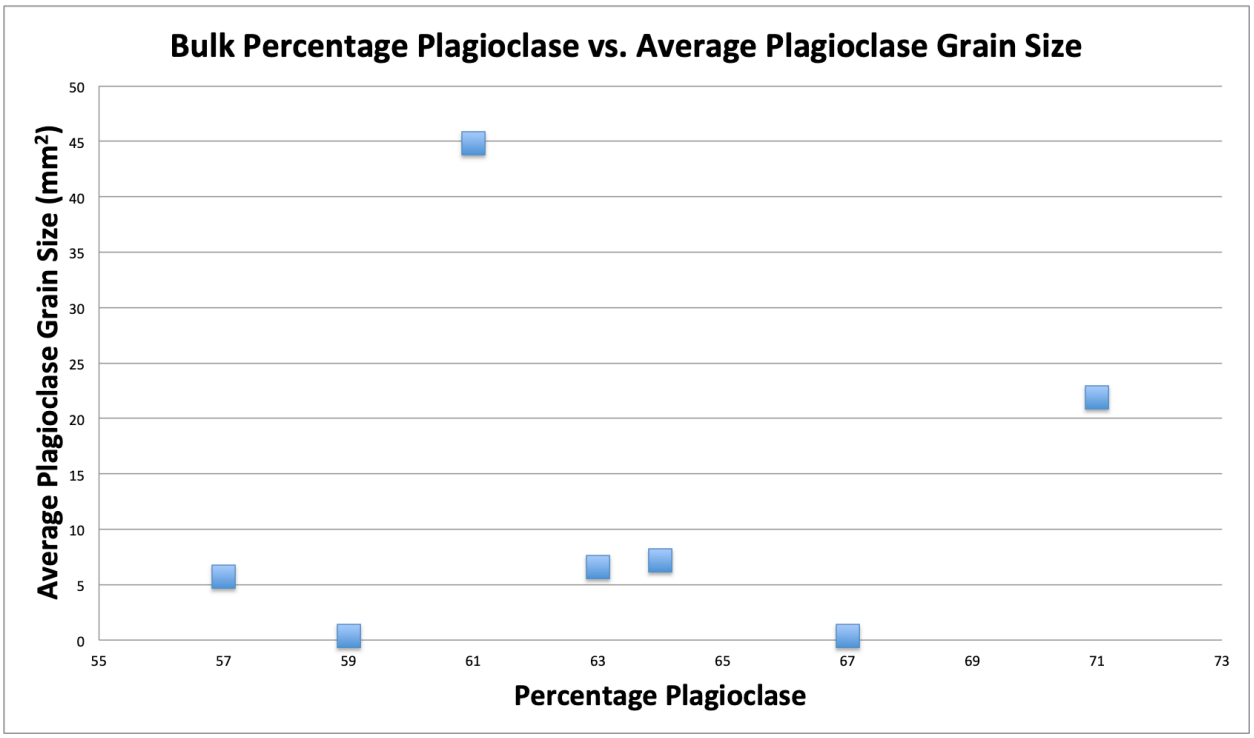

Figure 20. Graph showing bulk percentage of plagioclase, as compared to average plagioclase grain size, for each sample, as determined by point counting. There is no relationship between plagioclase grain size and mineralogy within each sample.

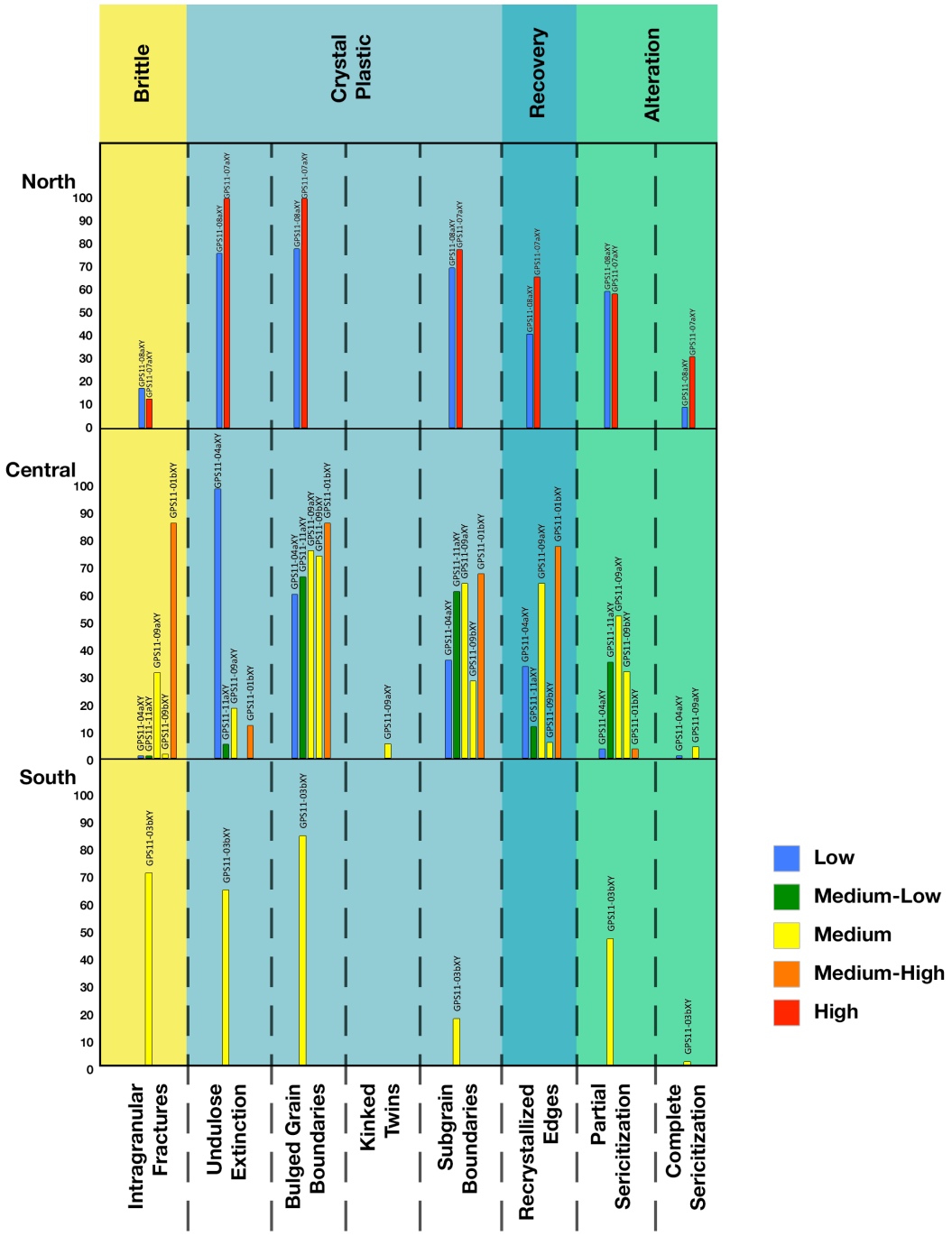

Figure 21. Plagioclase microstructures, grouped by interpreted deformation mechanism. These are separated into three regions, north, central and south. For all, the Y axis is the percentage occurrence plagioclase, the x axis are the observed microstructures, and the colored fields separate the inferred deformation mechanisms implied by the microstructures, the bar colors correspond to inferred strain at each site as determined by criteria listed in Table 2. Generally, crystal plastic deformation is the predominant mechanism throughout the GPS regardless of location or strain magnitude.

Chapter 5: Discussion

5.1 Controls on Shear Zone Formation

Overall, while the majority of exposures within the GPS contain shear zones which have accommodated deformation, there are two exposures which have deformed largely through pervasive foliation with very few shear zones (GPS11-08) or a complete absence of them (GPS11-04).

This variation in deformation style appears to be linked, at least in part, to grain size variation in the GPS, with finer grain sized lithologies favoring pervasive foliations and coarser grained lithologies favoring discrete shear zone formation. Through point counting, across all minerals, GPS11-04 has an average grain size of 0.2 mm^2, and GPS11-08 has an average grain size of 3.8 mm^2 (Table 2). GPS11-11 meanwhile, has an average grain size of 0.6 mm^2, but had deformation that was taken up by shear zones in addition to a moderate foliation. This would indicate that grain size, while important, is not the sole factor that determines shear zone formation. We hypothesize that overall strain at the exposure assisted in overcoming the fine grain size and allowed the development of shear zones.

5.2 Strain Patterns

Strain variation across the GPS is controlled more by localized variations and lithological controls than by other km scale features such as location within sill. Regionally strain did not vary systematically across or along the sill (Fig. 7). Field relationships indicate that there was great variation of grain size at some exposures, and when present, shear zones were preferentially located within the coarser grained regions, or occasionally localized at the boundary between the grain size variations.

5.3 Microstructures

Evidence of crystal plastic deformation (also known as dislocation creep), including undulose extinction, is found throughout all regions of the GPS. Bulged grain boundaries and subgrain boundaries, are the dominant microstructures; they are found in the majority of all plagioclase grains across all three regions. Previous studies indicate that for crystal plastic deformation to occur in feldspar, it must be deformed under moderate temperature conditions (>400°C; Passchier and Truow, 2005). This matches the conditions of amphibolite facies deformation interpreted for the region (500°C-600°C & ~3 kilobars pressure; Poulsen, 2000). Interestingly, signs of brittle deformation, specifically abundant intragranular fractures, are found in two of the 8 samples (03b & 01b), with significantly fewer of such features in the other six samples. The fractures indicate high strain rate, low temperature, or fluid infiltration during deformation (Vernon, 2004). A lack of major alteration in these samples makes fluid infiltration unlikely and metamorphic grade is relatively constant, suggesting that strain rates varied locally.

In sample 03b, the only sample from the southern region, there are no observed recrystallized edges and few subgrain boundaries, indicating a lack of recovery mechanisms. This may indicate that less recovery occurred. With dislocation creep serving as the dominant process throughout the GPS, the evidence for lesser recovery suggests a lower strain at this location.

Overall, it is clear that crystal plastic deformation is the primary deformation mechanism throughout the entirety of the GPS. There are some minor variations across the sill, such as lack of recovery in the south, but these are likely due to lower strain within that region or outcrop.

There appears to be no pattern regionally to the microstructures noted, nor directly related to strain variation.

5.4 Evolution of Shear Zones

Previous work had hypothesized that shear zones within the GPS initiated in a conjugate set with approximately 90° between each strand, and that through progressive deformation, the two strands rotated away from the shortening direction towards subparallel orientations (Carreras et al. 2010). This hypothesis has been tested using three outcrops from within the GPS: GPS11-03, GPS11-01, and GPS11-07 (Fig. 22). These three sites were chosen because: 1) they represent a variety of inferred qualitative strain, 2) they contained an adequate number of shear zones (n>10), and 3) they contained a large quantity of both thin and thick shear zones.

Across the three sites, the shortening direction angle between strands for both thin and thick sets was lowest in the least strained outcrop, highest in the highest strained, and had a value between these two in the middle strain. This pattern is consistent with the Carreras et al. (2010) model.

Within each site, old thick shear zone strands are rotated with respect to the younger thin shear zone strands in a way that is consistent with rotation away from the shortening direction. In GPS11-03 the thin strands have a separation angle of 69°, compared to 109° in the thick strands, with the dextral plane rotating counter-clockwise and the sinistral plane rotating clockwise. In GPS11-01 the thin strands have a separation angle of 92°, compared to 118° in the thick strands with the dextral plane rotating counter-clockwise and the sinistral plane rotating clockwise. Last, in GPS 11-07 the thin strands have a separation angle of 128°, compared to 156° in the older

strands with the dextral plane remaining in the same orientation and the sinistral plane rotating clockwise. These rotations are also consistent with the Carreras et al. (2010) model.

Additionally, the variation from thin to thick shear zones was analyzed for the three regions of the GPS, northern, central, and southern (Fig. 23). In the northern region the thin strands have a separation angle of 97°, compared to 152° in the thick strands, with the dextral plane rotating counter-clockwise and the sinistral plane rotating clockwise. In the central region, the thin strands have a separation angle of 83°, compared to 120° in the thick strands with both the dextral and sinistral plane rotating clockwise. Last, in the southern region the thin strands have a separation angle of 69°, compared to 109° in the older strands with the dextral plane rotating counter-clockwise and the sinistral plane rotating clockwise. All are consistent with the Carreras et al. (2010) model except for the sense of rotation of the dextral planes in the central region.

The shear zone orientation patterns from both of these sets of sites are consistent with the model proposed by Carreras et al. (2010). Increasing strain across the three sites shows an increase in the angle between strands. Additionally, within each individual site, and region, the thin, young shear zones have a lesser angle of separation between strands as compared to the thick, older strands, which further supports their evolution.

5.5 Shortening Direction

While the inferred shortening direction throughout the Grassy Portage sill varies, it is oriented consistently within a particular region. Generally, shortening is directed approximately NE/SW in the northern region, approximately NW/SE in the central region, and NW/SE in the southern region. These inferred shortening directions match those inferred from internal and

regional foliation, which also wrap around the Rice Bay Dome (assuming bulk shortening direction is perpendicular to foliation).

Within the northern region, four sites with a total of 42 shear zones with identifiable sense of motion were analyzed for inferred shortening orientation. The thin shear zones (35 measurements) have an inferred shortening direction of 040°/220°, with an angle of 97° between the sets. The thick shear zones (7 measurements) have an inferred shortening direction of 037°/217°, with an angle of 152° between them. Foliation was measured at 6 points in this region, and has an average strike of 122°/302°, which would infer a shortening direction from foliation alone of 032°/212°.

The central region is composed of seven sites, with a total of 117 shear zones with identifiable sense of motion. The thin shear zones (101 measurements) have an inferred shortening direction of 314°/134°, and an angle between sets of 83°. The thick shear zones (16 measurements) have an inferred shortening direction of 338°/158° and an angle between sets of 120°. Foliation was measured at 8 points in the region and has an average strike of 069°/249° and an inferred shortening direction of 339°/159°.

The southern region is represented by one site, encompassing 113 measured shear zones with identifiable sense of motion. The thin shear zones (107 measurements) have an inferred shortening direction of 159°/339°, and an angle between sets of 69°. The thick shear zones (6 measurements) have an inferred shortening direction of 164°/344° and an angle between sets of 114°. Foliation was measured once where it is oriented 084°/264°, indicating an inferred shortening direction of 174°/354°.

Looking at both the finite strain derived from fabric measurements and incremental strain derived from shear zone analysis, we see that within each of the three regions the implied

shortening direction is consistent. It is important to note that the shortening direction inferred from the foliation is the bulk finite shortened direction whereas the shortening direction inferred from the shear zones is an incremental shortening direction (the length of the increment depending on when the shear zones formed with respect to the overall strain). If the shortening directions inferred from each are subparallel, it means that either 1) the shear zones formed early in the deformation and record the bulk finite strain or 2) bulk strain was largely coaxial so that incremental and finite deformation have the same inferred shortening direction. The data indicate that the shortening direction from both fabric and shear zone orientations are nearly parallel. Regionally, the inferred shortening direction within the GPS varies significantly along its length. Previous work using deformation in dikes and veins in surrounding metavolcanic and metasedimentary rocks also shows that shortening directions vary in consistent patterns with the shortening directions found in this study (Fig. 24 ;Druguet et al. 2008). As the veins formed later in the D2 deformation, the consistent shortening direction with the GPS shear zones and foliation indicate that bulk deformation was nearly coaxial. Within both the GPS, and surrounding units, shortening direction varies systematically in relation to the Rice Bay Dome.

5.6 Curvature of GPS and shear zones

We have proposed two possible hypotheses to explain this variation in shortening direction along the length of the GPS:

1. The Rice Bay Dome is acting as a competent unit, surrounded by metavolcanic and metasedimentary units of lesser competence. The Rice Bay Dome is thus creating a regional scale “strain shadow,” deflecting the strain in the surrounding units and

creating variations in the strain direction, evidenced by the variations in shortening directions.

2. The current shear zones were formed during a period when the GPS was straight, rather than the current curved orientation wrapped around the RBD. In this scenario, when the shear zones formed, they all would have had the same geometries, and in turn the same inferred shortening orientation. Subsequently, after the formation of the shear zones, the entire GPS was folded around the RBD, resulting in the current geometrical variations.

When considering the first hypothesis, we can look toward analog and numerical modeling of rigid inclusions in lesser competent matrices to gain a better understanding. In numerical models, an applied bulk stress on a rigid inclusion resulted in the formation of perturbations in the stress and strain fields surrounding the inclusion, which varied in shape and location dependent upon the shape of the inclusion and orientation of the stress (Misra & Mandal, 2007). These results are further understood through analog studies where matrix materials are allowed to vary (Pascual et al. 2006). In a pure shear deformation experiment, a competent inclusion was placed in a multi-layered less competent matrix. This resulted in a complex folding of the matrix surrounding the inclusion, which varied dependent on the inclusion orientation and shape.

To consider the second hypothesis and better understand the curvature of the GPS and the orientations of its shear zones, the GPS was ‘uncurved’ to determine if the variation in orientations could be explained solely by subsequent curvature of the sill. First, each region was assigned an angle of orientation that best represented the orientation of the sill within it (Fig. 25). To determine the theoretical uncurved inferred shortening direction, the data for all regions was

rotated clockwise according to its representative angle: 125° for the north, 45° for the central, and 20° for the south.

Unfortunately, we currently do not know how exactly this curving would have occurred, and what the original orientation would have been. So "uncurving" parts of the GPS was done arbitrarily relative to an east-west reference orientation. As most of the GPS is steeply dipping, "uncurving" was only conducted about a vertical axis (changing the orientation of the strikes). Due to its lithology and contacts with surrounding metasedimentary and metavolcanic units, we can assume that the sill was flat lying prior to any deformation. As such, this test is solely to see if shear zones developed when the sill was straight rather than curved, i.e. if the curving of the unit alone could explain the shortening direction variation of the three regions.

Comparing stereographic projections of the three regions as measured in the field (Fig. 26) with those that are rotated (Fig.27) allows us to test this hypothesis. While the orientations themselves are not meaningful, as we do not know what the original orientation of the sill would have been, we can look at the differences between regional variations. For the thin shear zone sets, after uncurving, the central and southern shortening direction was exactly the same, and the northern shortening direction varied by 14° from them. The thick shear zone shortening direction had a variation of 41° total. Overall, these results are intriguing and show that the curvature of the GPS could reasonably account for the variation in shortening direction down the sill's length.

When evaluating the two hypotheses, both are reasonably consistent with the data collected from the GPS. Regional data may help with further evaluation.

5.7 Regional Deformation History

Like many units in the Rainy Lake region, the GPS has accommodated deformation differently than the surrounding units and the rest of the region. Discrete small shear zones have taken up the majority of deformation, although other factors including grain size and strain can lead to variations in the deformation style within the sill. Generally within the Rainy Lake region, deformation in weaker units such as metavolcanics and metasedimentary rocks is accommodated by pervasive foliation (Druguet et al., 2008; Czeck and Poulsen, 2010; Bauer et al., 2011). Deformation in stronger units such as the gneiss domes (Czeck and Poulsen, 2010; Bauer et al., 2011; Block, 2014) and the GPS is more likely to be accommodated by discrete shear zones bounding regions of lesser deformed rocks. As strain progresses, the bounded regions also become deformed as seen here in the more highly strained zones (Carreras et al., 2010).

The orientation of the shear zone strands is a viable indicator of the local strain orientation within the GPS and indicates that similar systematic variability in strain exists in the GPS and neighboring units (Druguet et al., 2008; Fig. 24). The Rice Bay Dome plays an important role in understanding the GPS and the shear zones within it. Both proposed hypotheses to explain the variation in shortening direction involve the Rice Bay Dome. It may have served as a competent unit around which lesser competent units have been wrapped, or alternatively its higher competence may have served to create a “strain shadow”, perturbing the strain imparted upon units located in close proximity to the dome.

Other regional data may help distinguish between these two hypotheses. All of the structural features we observe are broadly D2: foliation, shear zones in GPS, and deformation of veins from Druguet et al. (2008). However, some aspects of the map patterns are likely related to D1.

The GPS was likely emplaced into the volcanic and sedimentary package prior to deformation (2727 – 2728 Ma) (Davis et al. 1989). The tilting of these units into steep dips likely occurred during the D1 stacking phase of deformation (Poulsen, 2000; Poulsen and Czeck, 2010; Bauer et al., 2011), however the broad open folding around the Rice Bay Dome was a D2 feature (Poulsen et al., 1980; Poulsen, 2000). So the relative timing of features discussed here may be used to unravel the evolution of deformation during D2. The radiometric age of the late stage granites (orange colored units with cross pattern on map shown on Fig. 4) is 2686 ± 2 Ma (Davis et al. 1989; Fralick and Davis, 1999). Previous work suggested that these granites intruded very late in D2 (Czeck et al., 2006). The syn-D2 veins analyzed by Druguet et al. (2008) are likely to be of the same generation as the late stage granites. Since the systematic variation in shortening directions interpreted from those veins are compatible with the shortening directions interpreted from the GPS shear zones and the foliations, there is intriguing evidence to suggest that it is possible that D2 extended well after granite intrusion. The patterns of the northernmost part of the GPS and neighboring volcanics provide further supporting evidence, as they both curve around the Baseline Bay pluton (Fig. 5). This curving may have occurred in relation to or even after the intrusion of these late granitoids.

5.8 Regional Kinematics

While many authors have invoked transpression to describe features within the Rainy Lake Zone, the style of deformation and the kinematics of deformation vary throughout the heterogeneous rock units and bounding structures (Poulsen, 1986; Poulsen, 2000; Czeck and Hudleston, 2003; Druguet et al., 2008; Czeck et al., 2009; Carreras et al., 2010; Poulsen and Czeck, 2010; Bauer et al., 2011). In many examples, authors hypothesize that transpression was

partitioned into high strain zones dominated by simple shear and lower strain zones dominated by pure shear (e.g. Fossen et al., 1994; Curtis et al., 2010; Weinberger, 2014). There is evidence to suggest that the Rainy Lake Zone followed this general model with high strain simple shear concentrated at the discrete shear zone boundaries and more pure shear dominated transpression within the various units within the wedge (Bauer et al., 2011).

There is significant evidence to indicate that portions of the GPS may have been dominated by more pure shear dominant strain during deformation. Along the length of the GPS, the shortening direction inferred from both foliations and conjugate shear zones varies significantly and appears to wrap around the Rice Bay Dome located NW of the GPS (Fig. 24). In the northern and southern regions, the orientation of the inferred shortening and the rotation of shear zone limbs, as well as the nearly 1:1 ratio of dextral to sinistral shear zone occurrence (Fig. 14), are consistent with pure shear dominated deformation. Lastly, inferred shortening directions within the three regions are all approximately perpendicular to their corresponding regional foliation. If the shear zones formed during a later increment of D2 deformation, the coincidence of shortening directions interpreted from the shear zones and the foliation are consistent with pure shear dominated transpression.

a.

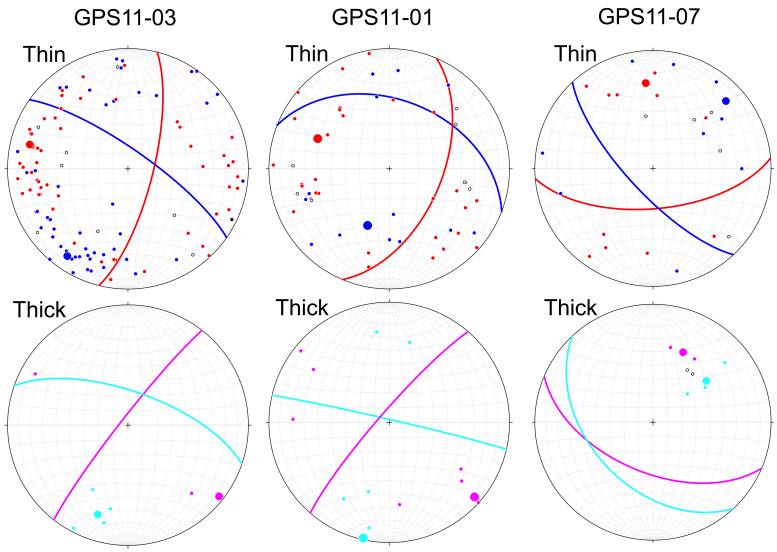

Site		GPS11-03	GPS11-01	GPS11-07
Qualitative Strain		Medium	Medium-High	High
Thin Shear Zone Average Orientatons	Dextral	305°	291°	317°
	Sinistral	014°	023°	085°
Angle Between Thin Sets		69°	92°	128°
Thick Shear Zone Average Orientatons	Dextral	289°	283°	317°
	Sinistral	038°	041°	113°
Angle Between Thick Sets		109°	118°	156°

b.

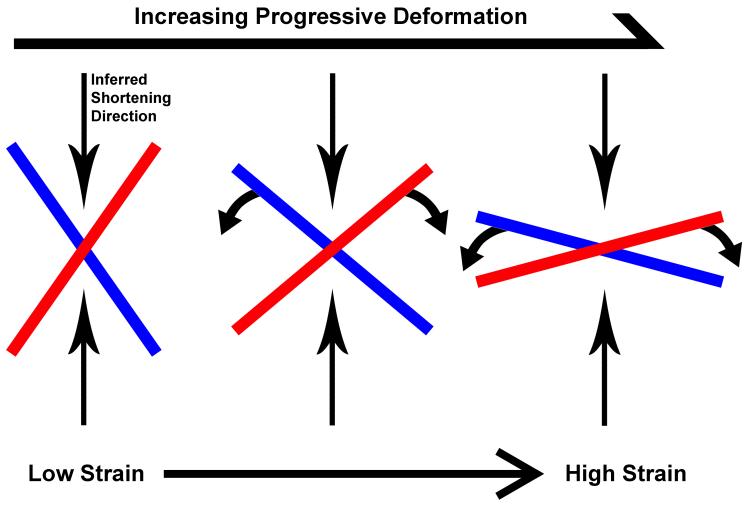

Figure 22. a) Stereographic projections for three outcrops within the GPS to show variation in shear zone orientation of thin and thick shear zone sets across three increasing amounts of qualitative strain. In all cases, the angle between the thick sets is larger than the angle between thin sets. For thin and thick sets, the angles increase with inferred relative outcrop strain. **b)** Schematic diagram of shear zone strands and the rotation of the average shear zone orientation away from the inferred shortening direction, through increasing progressive pure shear deformation. Blue are dextral shear zones and red are sinistral shear zones.

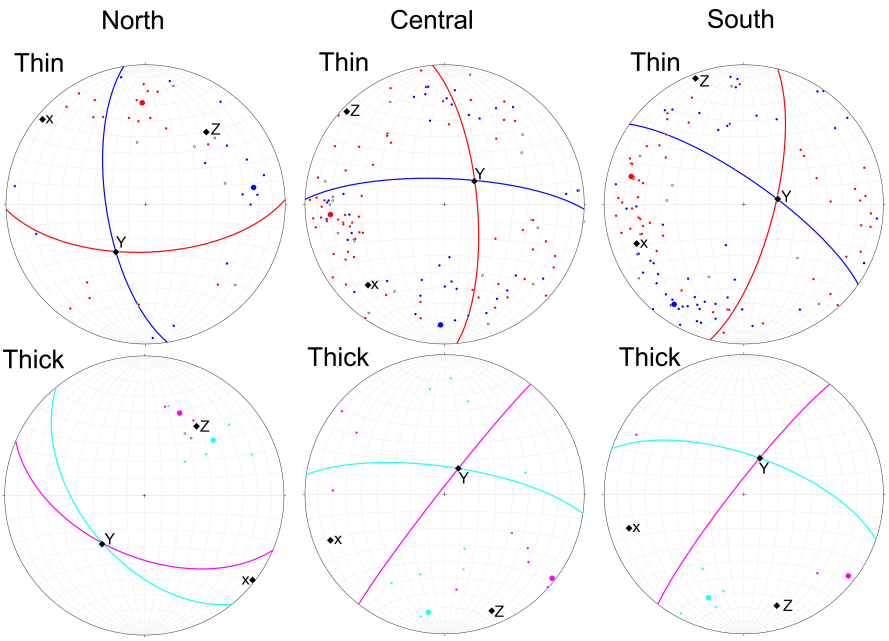

Region		Northern	Central	Southern
Thin Shear Zone Average Orientatons	Dextral	351°	272°	305°
	Sinistral	088°	355°	014°
Angle Between Thin Sets		97°	83°	69°
Thick Shear Zone Average Orientatons	Dextral	321°	278°	289°
	Sinistral	113°	038°	038°
Angle Between Thick Sets		152°	120°	109°

Figure 23. Stereographic projections for three regions within the GPS to show variation in shear zone strand orientation of thin and thick shear zone sets. In all cases, the angle between sets in thick shear zones is greater than the angle between sets in thin shear zones.

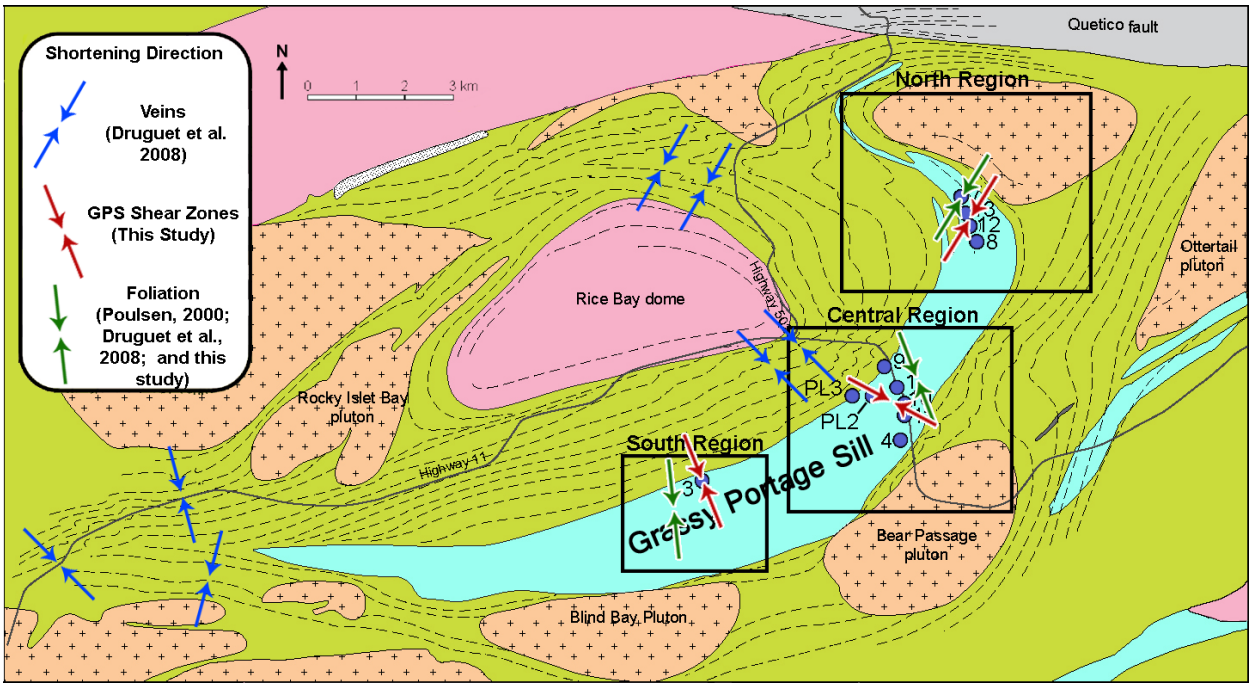

Figure 24. Generalized geologic map (based on Poulsen, 2000 and Druguet et al., 2008) with inferred shortening directions. Red arrows are regional inferred shortening based upon shear zone strand analysis, green arrows are inferred shortening based upon average regional foliation (from Poulsen, 2000 and Druguet et al., 2008), and blue arrows are approximate shortening directions from deformed veins as found in Druguet et al. 2008.

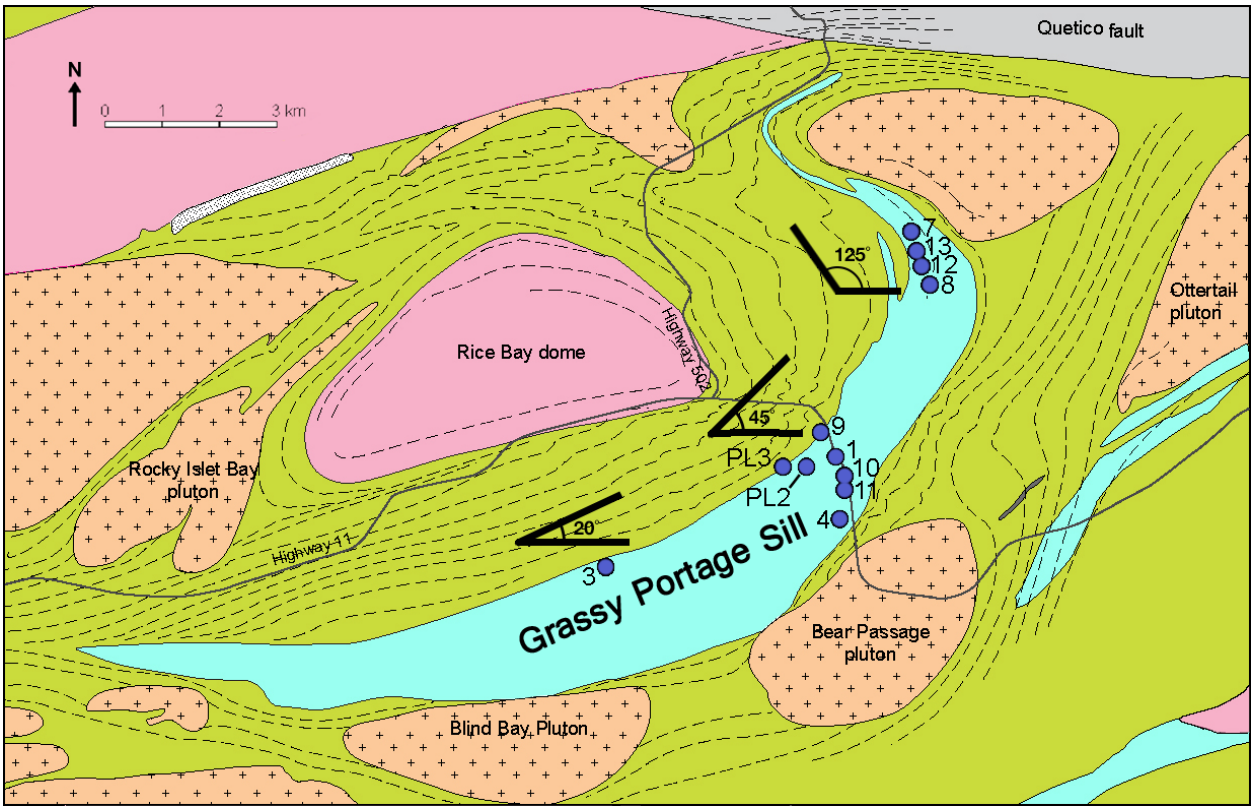

Figure 25. Generalized geologic map (based on Druguet et al., 2008) with the assumed general orientation of the GPS for each region. The angle shown is the angle used for rotation in the analysis shown in Figure 27. (Rotate to an arbitrary EW orientation).

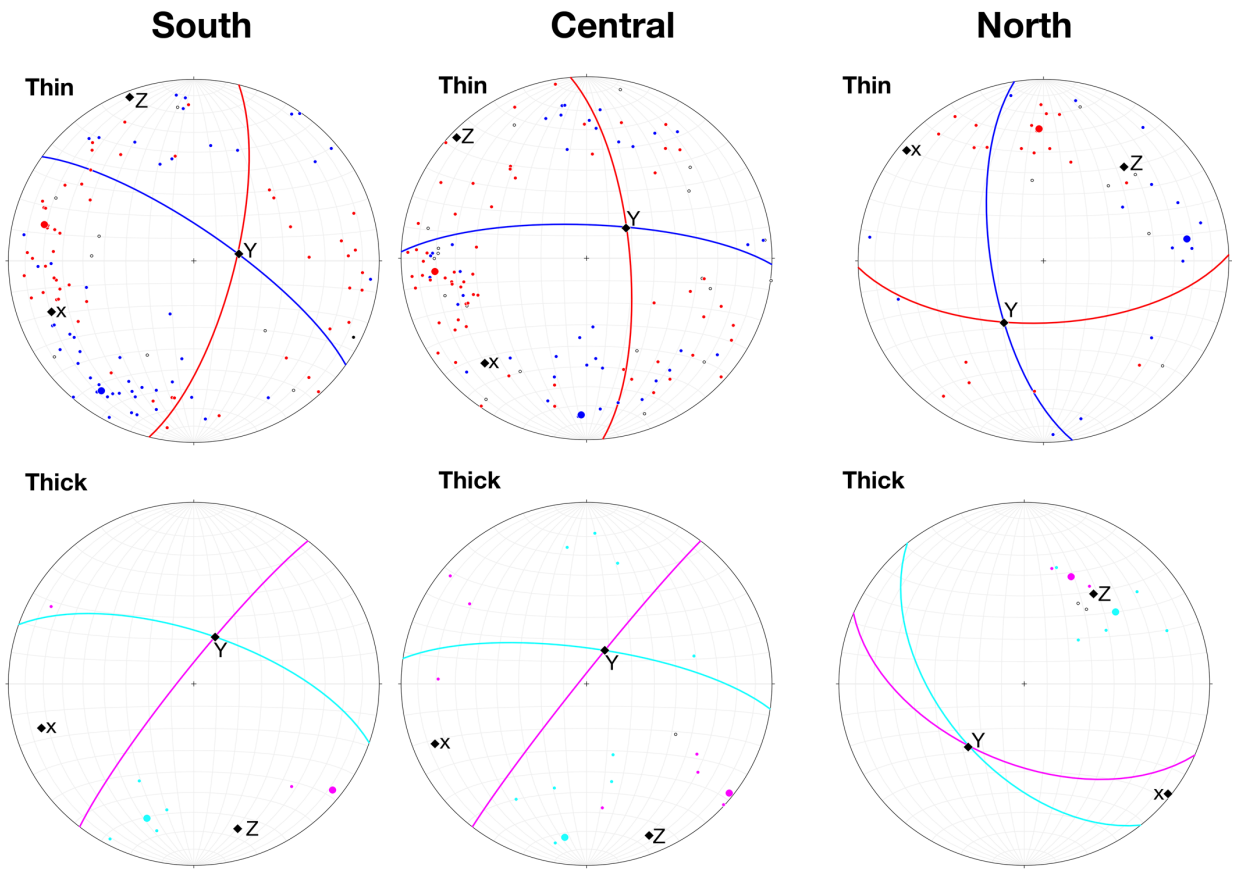

Figure 26. Stereographic Projections for both thick and thin shear zone sets for the three regions in their original orientations.

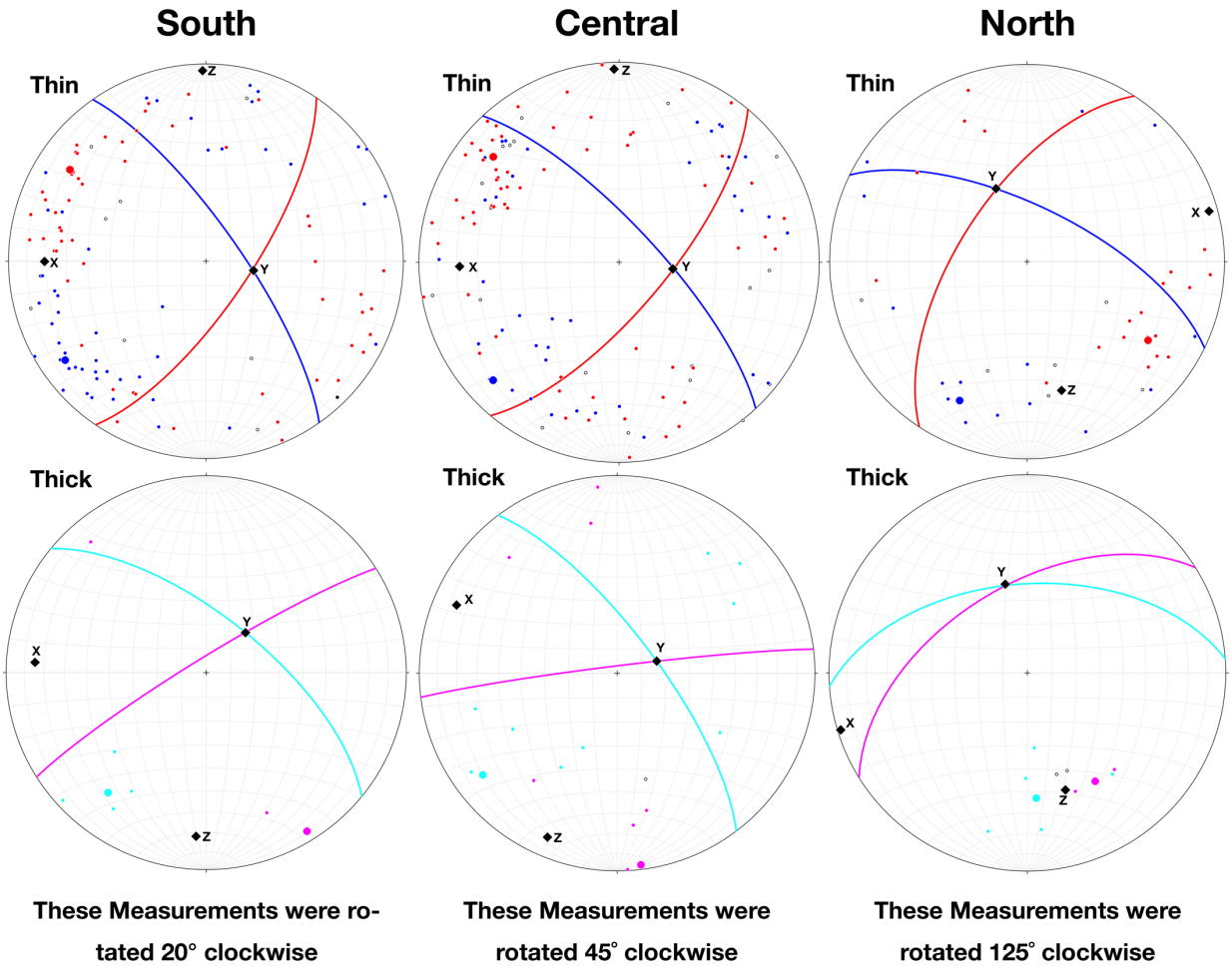

Figure 27. Resultant stereographic projections for both thick and thin shear zone sets for the three regions after rotation as determined by GPS orientation defined in figure 25.

Chapter 6: Conclusions

The Grassy Portage Sill, through deformation in the Kenoran orogeny, developed a complex network of anastomosing shear zones that evolved through progressive deformation. Through a detailed analysis of the shear zones and a study of the lithological and microstructural variations within the sill, the deformation can be better understood and placed within the regional deformational event.

1. Anastomosing shear zones have taken up the majority, though not all, of the deformation within the GPS. There are sections that accommodated deformation through development of pervasive foliation, or in some cases with a combination of pervasive foliation and discrete shear zone networks. This deformation style variation is linked to grain size and strain magnitude variation. Shear zones preferentially form in coarse-grained gabbros at high strain.
2. The inferred shortening directions from metamorphic fabric and conjugate shear zone geometries systematically vary along the sill. The variation in shortening direction mimics the shortening direction of surrounding rock units as determined by previous studies that used deformed veins as markers (Druguet et al. 2008). The local variation in shortening direction is related to deformation wrapping around the relatively rigid Rice Bay Dome. The consistency of shortening directions determined by various techniques and rock units suggest that the transpressional deformation was dominated by coaxial deformation.
3. Throughout the Rainy Lake zone, the complex terrane contains a variety of lithologies which have partitioned the deformation differently. The Grassy Portage Sill, unlike the

surrounding units, has primarily accommodated deformation through the network of conjugate shear zones.

4. The geometries of conjugate shear zones studied are consistent with previous models of shear zone development. Thin shear zones (≤1 cm) are assumed to be younger than thick (>1 cm) shear zones. Dextral and sinistral conjugate sets initiate at approximately 90° orientation and rotate in opposite directions away from the inferred shortening direction with increasing strain.
5. Crystal-plastic deformation, or dislocation creep, of plagioclase is the primary deformation mechanism across the GPS. Deformation mechanisms did not vary spatially or with strain throughout the sill.
6. To explain the variation in shortening direction along the length of the GPS, two distinct hypotheses were proposed: 1) The GPS was folded around the Rice Bay Dome, and shear zone development pre dated the folding event. 2) The high competence of the Rice Bay Dome caused deflections of the strain field around it which systematically varied the local shortening direction.
    a. For the first hypothesis, shear zones would have developed after D1 stacking but before major D2 folding, where the sill, along with surrounding units, were folded around the Rice Bay Dome. At a regional scale, the GPS appears to have been folded with influence from both the Rice Bay Dome (2725 ± 2 Ma) and the much younger Baseline Bay granite pluton (2686 ± 2 Ma). Previously, folding was interpreted to have occurred before the intrusion of these late plutons, but the data are also consistent with later folding, or folding over a longer period, with some overlap with the intrusion of the Baseline Bay

Pluton. Further analysis of other units within the region would be needed to better understand the likelihood of this hypothesis. Additionally, further study is needed to understand the original orientation of the sill during shear zone formation, perhaps through use of paleomagnetic data if there is a signal that can be attributed to original lithology and/or metamorphic fabrics.

b. For the second hypothesis, the highly competent Rice Bay Dome could have caused both the strain field perturbations, as well as the folding in surrounding units. Analog studies have shown that rigid inclusions within layered matrix will not only lead to strain field perturbations, but can also create folding patterns in the surrounding matrix that are unexpected as compared to deformation without the inclusion.

REFERENCES

Ackermann, R. V., Schlische, R. W.,1997. Anticlustering of small normal faults around larger faults. Geology 25, 1127– 1130.

Arbaret, L., Hussain, S., Dawood, H., Burg, J.-P., Zeilinger, G., Chaudhry, N., 2000. Pre-collisional anastomosing shear zones in the Kohistan arc, NW Pakistan. In: Khan, M.A., Treloar, P.J., Searle, M.P., Jan, M.Q. (Eds.), Tectonics of the Nanga Parbat Syntaxis and the Western Himalaya. Geological Society, London, Special Publications, vol. 170, pp. 295-311.

Arbaret, L., Burg, J.-P., 2003. Complex flow in lowest crustal, anastomosing mylonites: Strain gradients in a Kohistan gabbro, northern Pakistan, J. Geophys. Res., 108(B10), 2467, doi:10.1029/2002JB002295, 2003.

Baird, G. B., Hudleston, P. J., 2007. Modeling the influence of tectonic extrusion and volume loss on the geometry, displacement, vorticity, and strain compatibility of ductile shear zones. Journal of Structural Geology 29(10), 1665-1678.

Bauer, R.L., Czeck, D.M., Hudleston, P.J., Tikoff, B., 2011, Structural geology of the subprovince boundaries in the Archean Superior Province of northern Minnesota and adjacent Ontario, *in* Miller, J.D., Hudak, G.J., Wittkop, C., and McLaughlin, P.I., eds., Archean to Anthropocene: Field Guides to the Geology of the Mid-Continent of North America: Geological Society of America Field Guide 24, p. 203–241, doi:10.1130/2011.0024(10).

Bell, T.H., 1981. Foliation development: the contribution, geometry and significance of progressive, bulk, inhomogeneous shortening. Tectonophysics 75, 273-296.

Bhattacharyya, P., Czeck, D.M., 2008. Using network analyses within GIS technologies to quantify geometries of shear zone networks. Geosphere 4, 640-656.

Block, Jane, "The Rice Bay and Northeast Bay Gneiss Domes: a Kinematic Study of Competent Rock Bodies in the Rainy Lake Region of Ontario, Canada" (2014). Theses and Dissertations. Paper 395.

Borradaile, G. J., Dehls, J. F., 1993. Regional kinematics inferred from magnetic subfabrics in Archean rocks of northern Ontario, Canada. Journal of Structural Geology 15, 887-894.

Burg, J.-P., Ricou, L.-E., Ivanov, Z., Godfriaux, I., Dimov, D., Klain, L., 1996. Syn-metamorphic nappe complex in the Rhodope Massif: structure and kinematics. Terra Nova 8, 6-15.

Burg, J.-P., 1999. Ductile structures and instabilities: their implication for Variscan tectonics in the Ardennes. Tectonophysics, 309, 1–25.

Burg, J.-P & Arbaret, Laurent & Nawaz Chaudhry, Muhammad & Dawood, H & Hussain, S & Zeilinger, Gerold., 2005. Shear strain localization from the upper mantle to the middle crust of the Kohistan Arc (Pakistan). Geological Society, London, Special Publications. 245. 25-38. 10.1144/GSL.SP.2005.245.01.02.

Card, K.D., Ciesielski, A., 1986. DNAG subdivisions of the superior province of the Canadian shield. Geoscience Canada 13, 5-13.

Card, K. D., 1990. A review of the Superior Province of the Canadian Shield, a product of Archean accretion. Precambrian Research 48, 99-156.

Carreras, J., 2001. Zooming on northern Cap de Creus shear zones. Journal of Structural Geology 23, 1457-1486.

Carreras, J., Czeck, D.M., Druguet, E., and Hudleston, P.J., 2010, Structure and development of an anastomosing network of ductile shear zones: Journal of Structural Geology, v. 32, p. 656–666, doi:10.1016/j.jsg.2010.03.013.

Choukroune, P., Gapais, D., 1983. Strain pattern in the Aar granite (Central Alps): orthogneiss developed by bulk inhomogeneous flattening. Journal of Structural Geology 5, 411-418.

Christiansen, P. P. and Pollard, D. D. (1997) Nucleation, growth and structural development of mylonitic shear zones in granitic rocks. Journal of Structural Geology 19, 1159-1172.

Cobbold, P.R., Cosgrove, J.W., Summers, J.M., 1971. The development of internal structures in deformed anisotropic rocks. Tectonophysics 12, 23-53.

Corsini, M., Vauchez, A., Caby, R., 1996. Ductile duplexing at a bend of a continental- scale strike-slip shear zone: example from NE Brazil. Journal of Structural Geology 18, 385-394.

Curtis, M.L., Flowerdew, M.J., Riley, T.R., Whitehouse, M.J., Daly, J.S., 2010. Andean sinistral transpression and kinematic partitioning in South Georgia. Journal of Structural Geology 32, 464-477.

Czeck, D.M., Hudleston, P.J., 2003. Testing models for obliquely plunging lineations in transpression: a natural example and theoretical discussion. Journal of Structural Geology 25, 959-982.

Czeck, D.M., Hudleston, P.J., 2004. Physical experiment of vertical transpression with localized nonvertical extrusion. Journal of Structural Geology 26, 573-581.

Czeck, D.M., Maes, S.M., Sturm, C.L., Fein, E.M., 2006. Assessment of the relationship between emplacement of the Algoman plutons and regional deformation in the Rainy Lake region, Ontario. Canadian Journal of Earth Sciences 43, 1651-1653.

Czeck, D. M. and Poulsen, K. H., 2010. Field trip guide: Deformation in the Rainy Lake Region: A Fabulous Display of Structures Controlled by Rheological Contrasts. Institute on Lake Superior Geology 56th Annual Meeting, International Falls, MN, 2010; 56 Part 2, 47-75.

Czeck, D.M., Fissler, D.A., Horsman, E., and Tikoff, B., 2009, Strain analysis and rheology contrasts in polymictic conglomerates: An example from the Seine metaconglomerates, Superior Province, Canada: Journal of Structural Geology 31, p. 1365–1376, doi:10.1016/j.jsg.2009.08.004.

Czeck, D. M., Fralick, P., 2002. Field trip 3: Structure and sedimentology of the Seine Conglomerate, Mine Centre area, Ontario. Proceedings and Abstracts - Institute on Lake Superior Geology 48, Part 1, 37-67.

Davis, D.W., Poulsen, K.H., Kamo, S.L., 1989. New insights into Archean crustal development from geochronology in the Rainy Lake area, Superior Province, Canada. Journal of Geology 97, 379-398.

Druguet, E., Czeck, D.M., Carreras, J., Castaño, L.M., 2008. Emplacement and deformation features of syntectonic leucocratic veins from Rainy Lake zone (Western Superior Province, Canada). Precambrian Research 163, 384-400.

Fernández, C., Czeck D.M., Díaz-Azpiroz, M., 2013. Testing the model of oblique transpression with oblique extrusion in two natural cases: steps and consequences. Journal of Structural Geology 54, 85–102.

Fusseis, F., Handy, M.R., Schrank, C., 2006. Networking of shear zones at the brittle- to-viscous transition (Cap de Creus, NE Spain). Journal of Structural Geology 28, 1228-1243.

Fossen, H. (2010). *Structural geology*. Cambridge: Cambridge University Press.

Fossen, H., Cavalcante, G.C.G., 2017. Shear zones – A review. Earth-Sci. Rev. 171, 434–455.

Fossen, H., Tikoff, B., Teyssier, C. T., 1994. Strain modeling of transpressional and transtensional deformation. Norsk Geologisk Tidsskrift 74, 134-145.

Fralick, P., Davis, D., 1999. The Seine-Coutchiching problem revisited: sedimentology, geochronology and geochemistry of sedimentary units in the Rainy Lake and Sioux Lookout Areas. In: Harrap, R. M. & Helmstaedt, H. (Ed.), 1999 Western Superior Transect Fifth Annual Workshop 70. Lithoprobe Secretariat, University of British Columbia, 66-75.

Fusseis, F., Handy, M.R., Schrank, C., 2006. Networking of shear zones at the brittle- to-viscous transition (Cap de Creus, NE Spain). Journal of Structural Geology 28, 1228-1243.

Gapais, D., Bale, P., Choukroune, P., Cobbold, P.R., Mahjoub, Y., Marquer, D., 1987. Bulk kinematics from shear zone patterns: some field examples. Journal of Structural Geology

9, 635-646.

Goncalves, P., Poilvet, J.-C., Oliot, E., Trap, P., Marquer, D., 2016. How does shear zone nucleate? An example from the Suretta nappe (Swiss Eastern Alps). J. Struct. Geol. 86, 166–180.

Hobbs, B.E., Mülhaus, H.B., Ord, A., 1990. Instability, softening and localization of deformation. Geol. Soc. Spec. Publ. 54, 143–165.

Hoffman, P. F., 1989. Precambrian geology and tectonic history of North America. In: Bally, A. W., Palmer, A. R. (Eds.), The geology of North America; an overview. The geology of North America A, pp. 447-512.

Hudleston, P., 1999. Strain compatibility and shear zones: is there a problem? Journal of Structural Geology 21, 923-932.

Hull, J., 1988. Thickness-displacement relationships for deformation zones. J. Struct. Geol. 4, 431–435.

Ingles, J., Lamouroux, C., Soula, J.-C., Guerrero, N., Debat, P., 1999. Nucleation of ductile shear zones in a granodiorite under greenschist facies conditions, Ne´ovielle massif, Pyrenees, France, Journal of Structural Geology 21, 555 – 576.

Langford, F. F., Morin, J. A., 1976. The development of the Superior Province of northwestern Ontario by merging island arcs. American Journal of Science 276, 1023-1034.

Lawson, A. C., 1887. Geology of the Rainy Lake region, with remarks on the classification of the Crystalline Rocks west of Lake Superior. Preliminary note. American Journal of Science 33, 473-480.

Lawson, A. C., 1913. The Archaean geology of Rainy Lake re-studied. Memoir - Geological Survey of Canada 40.

Maerten, L., Gillespie, P., Pollard, D. D., 2002. Effect of local stress perturbation on secondary fault development. Journal of Structural Geology 24, 145-153.

Mancktelow, N.S., 2002. Finite-element modelling of shear zone development in viscoelastic materials and its implications for localisation of partial melts. Journal of Structural Geology 24, 1045-1053.

Mancktelow, N. S., 2006. How ductile are ductile shear zones? Geology, 34, 345–348, doi:10.1130/G22260.1.

Mandal, N., Misra, S., Samanta, S.K., 2004. Role of weak flaws in nucleation of shear zones: an experimental and theoretical study. J. Struct. Geol. 26, 1391–1400.

Means, W.D., 1995. Shear zones and rock history. Tectonophysics 247, 157–160.

Misra, S., Mandal, N., 2007. Localization of plastic zones in rocks around rigid inclusions: insights from experimental and theoretical models. J. Geophys. Res. 112, 15.

Mitra, G., 1979. Ductile deformation zones in Blue Ridge basement rocks and estimation of finite strain. Geological Society of America Bulletin 90, 935-951.

Mitra, G., 1998. Anastomosing deformation zones. In: Snoke, A.W., Tullis, J., Todd, V. R. (Eds.), Fault-related Rocks: a Photographic Atlas. Princeton University Press, pp. 142-143.

Passchier, C.W., Trouw, R.A.J., 2005. Microtectonics, second ed. Springer-Verlag, Berlin, 366 pp.

Pennacchioni, G., 2005. Control of the geometry of precursor brittle structures on the type of ductile shear zone in the Adamello tonalites, Southern Alps (Italy). Journal of Structural Geology 27, 627–644.

Pennacchioni, G., Mancktelow, N. S., 2007. Nucleation and initial growth of a shear zone network within compositionally and structurally heterogeneous granitoids under amphibolite facies conditions. Journal of Structural Geology 29, 1757–1780.

Percival, J. A., Williams, H. R., 1989. Late Archean Quetico accretionary complex, Superior province, Canada. Geology 17, 23-25.

Ponce, C., Druguet, E., Carreras, J., 2013. Development of shear zone-related lozenges in foliated rocks. Journal of Structural Geology 50, 176–186.

Poulsen, K.H., 2000a. Archean metallogeny of the Mine Centre - Fort Frances area. Ontario Geological Survey Report 266.

Poulsen, K. H., 1986. Rainy Lake Wrench Zone: An example of an Archean Subprovince boundary in Northwestern Ontario. In: de Wit, M. J., Ashwal, L. D. (Eds.), Tectonic evolution of greenstone belts Technical Report 86-10, pp. 177-179.

Poulsen, K.H., Borradaile, G.J., Kehlenbeck, M.M., 1980. An inverted Archean succession at Rainy Lake, Ontario. Canadian Journal of Earth Sciences 17, 1358-1369.

Ramsay, J.G., Huber, M.I., 1983. The Techniques of Modern Structural Geology: Strain Analysis. 1 Academic Press, London (307 pp.).

Ramsay, J.G., Allison, I., 1979. Structural analysis of shear zones in an Alpinised Hercynian granite, Maggia Nappen, Pennine zone, Central Alps. Schweizer Mineralogische und Petrographische Mitteilungen 59, 251-279.

Ramsay, J.G., Graham, R.H., 1970. Strain variations in shear belts. Canadian Journal of Earth Sciences 7, 786-813.

Schrank, C.E., Boutelier, D.A., Cruden, A.R., 2008. The analogue shear zone: from rheology to associated geometry. Journal of Structural Geology 30, 177-193.

Segall, P., Pollard, D. D., 1983. Nucleation and growth of strike slip faults in granite. Journal of Geophysical Research 88, 555-568.

Stone, D., Hallé, J., Murphy, R., 1997a. Precambrian geology, Mine Centre area. Ontario Geological Survey Preliminary Map P. 3372, scale 1:50,000.

Stone, D., Hallé, J., Murphy, R., 1997b. Precambrian geology, Mine Centre area. Ontario Geological Survey Preliminary Map P. 3373, scale 1:50,000.

Vernon, R.H., 2004. A Practical Guide to Rock Microstructure. Cambridge University Press, Cambridge.

Weinberger, R., 2014. Pleistocene Strain Partitioning During Transpression Along the Dead Sea Transform, Metulla Saddle, Northern Israel. Dead Sea Transform Fault System: Reviews, 151-182.

Wilcox, R.E., Harding, T.P., Seely, D.R., 1973. Basin wrench tectonics. The American Association of Petroleum Geologists Bulletin 57, 74-96.

Wood, J., Dekker, J., Jansen, J. G., Keay, J. P., Panagapko, D., 1980a. Mine Centre Area (Eastern Half), District of Rainy River. Ontario Geological Survey Preliminary Map P. 2202, scale 1:15840.

Wood, J., Dekker, J., Jansen, J. G., Keay, J. P., Panagapko, D., 1980b. Mine Centre Area (Western Half), District of Rainy River. Ontario Geological Survey Preliminary Map P. 2201, scale 1:15840.